

RESEARCH ARTICLE

The single *Marchantia polymorpha* FERONIA homolog reveals an ancestral role in regulating cellular expansion and integrity

Martin A. Mecchia^{1,§}, Moritz Rövekamp^{1,*;§}, Alejandro Giraldo-Fonseca¹, Dario Meier¹, Philippe Gadiet^{1,‡}, Hannes Vogler¹, Daria Limacher¹, John L. Bowman² and Ueli Grossniklaus^{1,¶}

ABSTRACT

Plant cells are surrounded by a cell wall, a rigid structure that is not only important for cell and organ shape, but is also crucial for intercellular communication and interactions with the environment. In the flowering plant *Arabidopsis thaliana*, the 17 members of the *Catharanthus roseus* RLK1-like (*CrRLK1L*) receptor kinase family are involved in a multitude of physiological and developmental processes, making it difficult to assess their primary or ancestral function. To reduce genetic complexity, we characterized the single *CrRLK1L* gene of *Marchantia polymorpha*, *MpFERONIA* (*MpFER*). Plants with reduced *MpFER* levels show defects in vegetative development, i.e. rhizoid formation and cell expansion, and have reduced male fertility. In contrast, cell integrity and morphogenesis of the gametophyte are severely affected in *Mpfer* null mutants and *MpFER* overexpression lines. Thus, we conclude that the *CrRLK1L* gene family originated from a single gene with an ancestral function in cell expansion and the maintenance of cellular integrity. During land plant evolution, this ancestral gene diversified to fulfill a multitude of specialized physiological and developmental roles in the formation of both gametophytic and sporophytic structures essential to the life cycle of flowering plants.

KEY WORDS: Cell wall integrity, Cell elongation, *CrRLK1L* receptor kinases, *Marchantia polymorpha*, Signaling pathway evolution

INTRODUCTION

The functioning of plant cells is contingent upon the cell wall acting as a barrier between the cell and its environment. This complex matrix of polysaccharides, glycoproteins and other organic compounds defines the growth and shape of a cell and provides protection against biotic and abiotic stresses (Zhu et al., 2021; Showalter, 1993; Franck et al., 2018). Moreover, the cell wall has to resist turgor pressure while also allowing cell expansion during growth. Thus, sensing and controlling cell wall integrity (CWI) is crucial for plant cells, and receptor kinases (RKs) play an important role in sensing extracellular cues that activate intracellular pathways. Different RK subfamilies are defined by their extracellular domain (ECD), which is more variable than their

transmembrane and kinase domains (Shiu and Bleecker, 2001). Over the last decade, the *Catharanthus roseus* RLK1-like (*CrRLK1L*) subfamily emerged as important CWI sensors (Steinwand and Kieber, 2010; Wolf et al., 2012).

Functions have been assigned to 15 of the 17 *CrRLK1L* members encoded in the *Arabidopsis thaliana* genome: they are required for sensing environmental cues and cell-cell communication in diverse contexts, including reproduction, hormone signaling, cell expansion, innate immunity and various stress responses (Escobar-Restrepo et al., 2007; Hématy et al., 2007; Boisson-Dernier et al., 2009; Guo et al., 2009a,b; Kessler et al., 2010; Bai et al., 2014; Schoenaers et al., 2018; Miyazaki et al., 2009; Keinath et al., 2010; Duan et al., 2010; Galindo-Trigo et al., 2020; Zhu et al., 2018; Li et al., 2015; Richter et al., 2017, 2018; Stegmann et al., 2017). For instance, *FERONIA* (*AtFER*), *THESEUS1* (*AtTHE1*), *HERCULES1* (*AtHERK1*) and *AtHERK2* are required for cell elongation as *Atfer* single, *Atthe1 Atherk1* double, and *Atthe1 Atherk1 Atherk2* triple mutants exhibit stunted growth (Hématy et al., 2007; Guo et al., 2009a,b; Kessler et al., 2010). Root hairs burst in mutants in which *AtFER* and *[Ca²⁺]_{cyt}-ASSOCIATED PROTEIN KINASE1* (*AtCAP1*) [also known as *ERULUS* (*AtERU*)] are affected (Bai et al., 2014; Duan et al., 2010). Moreover, *AtFER* plays a role in powdery mildew resistance (Kessler et al., 2010), innate immunity (Keinath et al., 2010; Stegmann et al., 2017), calcium signaling (Ngo et al., 2014), phytohormone signaling (Guo et al., 2009b; Yu et al., 2012; Mao et al., 2015; Deslauriers and Larsen, 2010), and mechano- and heavy metal sensing (Richter et al., 2017; Shih et al., 2014). In most contexts, the *CrRLK1L*s tend to promote cellular growth and cell elongation. In contrast, *AtTHE1* actively inhibits cell elongation in hypocotyls when cell wall perturbations occur, e.g. as a result of mutations in the cell wall biosynthesis machinery or upon treatment with isoxaben, a cellulose synthesis inhibitor (Hématy et al., 2007; Denness et al., 2011).

In addition to regulating cellular growth during the vegetative phase of the life cycle, several *CrRLK1L*s play a role during fertilization by controlling the growth and reception of the pollen tube. In the female gametophyte, *AtFER* is highly expressed in the two synergid cells that flank the egg cell and are important for double fertilization (Escobar-Restrepo et al., 2007; Okuda et al., 2009). *AtFER* is crucial for pollen tube reception and the release of the two sperm cells (Escobar-Restrepo et al., 2007; Guo et al., 2009b; Ngo et al., 2014; Huck et al., 2003; Rotman et al., 2003), a process also involving two other, redundantly acting synergid-expressed *CrRLK1L*s, *AtHERK1* and *ANJEA* (*AtANJ*) (Galindo-Trigo et al., 2020). Moreover, *AtFER* and *AtANJ* also play a role in pollen-stigma recognition during pollen germination (Zhu et al., 2021). In contrast to these synergid-expressed *CrRLK1L*s, four pollen-expressed *CrRLK1L*s, named *ANXURI* (*AtANX1*), *AtANX2*, *BUDDHAS PAPER SEAL1* (*AtBUPS1*) and *AtBUPS2* (Boisson-Dernier et al., 2009; Miyazaki et al., 2009;

¹Department of Plant and Microbial Biology and Zurich-Basel Plant Science Center, University of Zurich, 8008 Zurich, Switzerland. ²The School of Biological Sciences, Monash University, Clayton, Melbourne, Victoria 3800, Australia.

*Present address: Kantonsschule Uetikon am See, 8708 Uetikon am See, Switzerland.

‡Present address: Institute of Molecular Plant Science, University of Edinburgh, Daniel Rutherford Building, Max Born Crescent, Edinburgh EH9 3BF, UK.

§These authors contributed equally to this work

¶Author for correspondence (grossnik@botinst.uzh.ch)

© M.A.M., 0000-0002-3444-3294; M.R., 0000-0001-6989-9104; A.G.-F., 0000-0001-7251-8245; H.V., 0000-0002-6552-4708; J.L.B., 0000-0001-7347-3691; U.G., 0000-0002-0522-8974

Zhu et al., 2018; Ge et al., 2017), are redundantly required for pollen tube integrity and tip growth.

To transduce extracellular cues, *CrRLK1L*s bind secreted peptides of the RAPID ALKALINIZATION FACTOR (RALF) family (Stegmann et al., 2017; Ge et al., 2017; Haruta et al., 2014; Dünser et al., 2019; Xiao et al., 2019), which induce complex formation with members of LORELEI (LRE) family of GPI-anchored proteins to signal to the interior of the cell (Ge et al., 2017; Xiao et al., 2019; Mecchia et al., 2017; Capron et al., 2008). Hence, it was suggested that at least some *CrRLK1L*s act as CWI sensors that coordinate cell elongation in response to changes in the cell wall (Boisson-Dernier et al., 2011; Hématy and Höfte, 2008; Cheung and Wu, 2011; Nissen et al., 2016; Feng et al., 2018; Lindner et al., 2012). A role as CWI sensors is also consistent with recent findings that AtFER interacts with pectin (Feng et al., 2018; Tang et al., 2021; Lin et al., 2021).

The 17 *A. thaliana* *CrRLK1L*s act partially redundantly and sometimes even have opposite effects on cellular growth (reviewed by Li et al., 2015; Nissen et al., 2016; Lindner et al., 2012; Galindo-Trigo et al., 2016). To investigate the original function of *CrRLK1L*s, we characterized them in a system with reduced genetic complexity: the liverwort *Marchantia polymorpha*, the genome of which encodes only one *CrRLK1L* (Bowman et al., 2017; Rövekamp et al., 2014). Liverworts represent an early diverging land plant lineage and have been hypothesized to retain, at least in part, characteristics of the earliest land plants (Bowman et al., 2017, 2007; Nishiyama et al., 2003; Qiu et al., 2006; Wickett et al., 2014; Mishler and Churchill, 1984; Kenrick and Crane, 1997). The presence of similar types of gene families in all plant lineages suggests that the differences in development evolved by co-opting and modifying existing developmental programs and genetic networks, rather than through the evolution of novel genes (Bowman et al., 2007; Nishiyama et al., 2003; Floyd and Bowman, 2007). *M. polymorpha* is thus an ideal system in which to study the ancestral role of genes and how it was modulated and diversified during land plant evolution (Bowman et al., 2017, 2016; Ishizaki, 2017).

We refer to the single *CrRLK1L* encoded in the *M. polymorpha* genome, Mp4g15890 (Mapoly0869s0001), as MpFERONIA (MpFER) (Galindo-Trigo et al., 2016; Bowman et al., 2017; Rövekamp et al., 2014) [also known as MpTHESEUS (MpTHE)] (Honkanen et al., 2016). An Mpfer mutant was identified in a large T-DNA screen for defective rhizoid formation, developing short and irregularly shaped rhizoids with brown tips, indicating rhizoid rupture (Honkanen et al., 2016). In the same screen, a mutant affecting the ortholog of the *A. thaliana* receptor-like cytoplasmic kinase MARIS (AtMRI), known to act downstream of AtFER, was identified with a similar phenotype [named Mpmri or Mppti; Mp7g17560 (Mapoly0051s0094)] (Honkanen et al., 2016; Westermann et al., 2019). As in *A. thaliana*, a dominant active version of MpMRI can partially rescue the Mpfer rhizoid phenotype (Westermann et al., 2019). This suggests that at least some of the machinery associated with cell elongation and CWI sensing is conserved between *A. thaliana* and *M. polymorpha*.

Here, we report that MpFER function is required for a variety of aspects of *M. polymorpha* gametophyte development. Phylogenetic analyses suggest that *CrRLK1L* genes first appeared in the common ancestor of land plants. The characterization of lines with reduced MpFER levels indicates that, in addition to its function in rhizoid formation, MpFER controls cell size and organ growth and is involved in male gametogenesis and fertility. Analysis of the MpFER expression pattern points to an involvement in female sexual organogenesis and sporophyte development. Our data suggest that the broad involvement of *CrRLK1L* function in the

development and physiology of land plants is an ancestral and conserved characteristic, although the functions of *CrRLK1L*s were extended and adapted to control additional developmental processes in the sporophyte during the course of land plant evolution.

RESULTS

CrRLK1L is conserved in land plants and arose in this lineage

The *M. polymorpha* genome encodes a single *CrRLK1L* homolog [Mp4g15890 (Mapoly0869s0001)] (Galindo-Trigo et al., 2016; Bowman et al., 2017; Rövekamp et al., 2014). Like other *CrRLK1L* members, this gene encodes an intracellular serine/threonine kinase domain, a transmembrane domain and an extracellular malectin-like domain with two malectin domains (Fig. 1A). Given that the ECD of *CrRLK1L*s in *A. thaliana* is crucial for their function and, in contrast to the kinase domain, not interchangeable (Kessler et al., 2014), we performed a phylogenetic analysis with the amino acid sequences of the predicted malectin-like domain of Mp4g15890, the *CrRLK1L*s of the mosses *Physcomitrium patens* (five members), *Sphagnum fallax* (seven members) and *Ceratodon purpureus* (three members), the hornworts *Anthoceros agrestis* Bonn (one member), *Anthoceros agrestis* Oxford (one member) and *Anthoceros punctatus* (one member), the lycophyte *Selaginella moellendorffii* (two members), the basal angiosperm *Amborella trichopoda* (nine members) and the 17 *CrRLK1L*s of *A. thaliana* (Fig. 1B). The *M. polymorpha* *CrRLK1L* member grouped together with the *CrRLK1L*s of basal land plants and was in the same clade as, for example, AtFER, AtHERK2 and AtANX1/2, whereas AtTHE1 was in a different one (Fig. 1B). Based on this phylogenetic position and the fact that the malectin-like domain of the *M. polymorpha* *CrRLK1L* shared the highest amino acid identity with AtFER (Fig. S1A), we named it MpFER (Bowman et al., 2017; Rövekamp et al., 2014; Westermann et al., 2019).

Interestingly, no significant similarity to the MpFER malectin-like domain was found among available genomic data of six Chlorophyte algae (*Chlamydomonas reinhardtii*, *Dunaliella salina*, *Volvox carteri*, *Coccomyxa subellipsoidea*, *Micromonas pusilla*, *Ostreococcus lucimarinus*) and expression data of six Charophyte algae (*Klebsormidium nitens*, *Nitella mirabilis*, *Coleochaete orbicularis*, *Spirogyra pratensis*, *Mesostigma viride*, *Closterium peracerosum–strigosum–littorale* complex). In the *Closterium* complex, an RK named CpRLK1 expressed during sexual reproduction was suggested to be a *CrRLK1L* homolog (Hirano et al., 2015). However, comparing the full sequence or the ECD of CpRLK1 with the predicted *M. polymorpha* proteome, higher identity to another RK was found [Mp1g17720 (Mapoly0001s0111)] (Fig. S1B,C). Moreover, no RALF orthologs have been reported in algae, suggesting the origin of the *CrRLK1L* pathway in land plants (Bowman et al., 2017). A similar conclusion was recently reached by analyzing the RALF family in *P. patens* (Ginanjar et al., 2021). Moreover, the best candidate obtained by BLAST analysis using the MpFER malectin-like domain against the genome of the Charophyte alga *Chara braunii* clustered outside the *CrRLK1L* phylogenetic tree (Fig. 1B, Fig. S1B).

To support MpFER as a member of the *CrRLK1L* subfamily, the 3D structure of its ECD was modeled (Schwede et al., 2003) using the structure of the AtFER ECD (PDB 6a5b.1A; Xiao et al., 2019) as a template (Fig. 1C). Overall, the predicted structure of the MpFER ECD is highly similar to that of AtFER, keeping an almost identical number of secondary structures [seven α -helices and 33 β -sheets in the MpFER ECD (Xiao et al., 2019) and eight α -helices and 34 β -sheets in the AtFER ECD, respectively], and a similar spatial disposition for 32 of the β -sheet structures and six of the

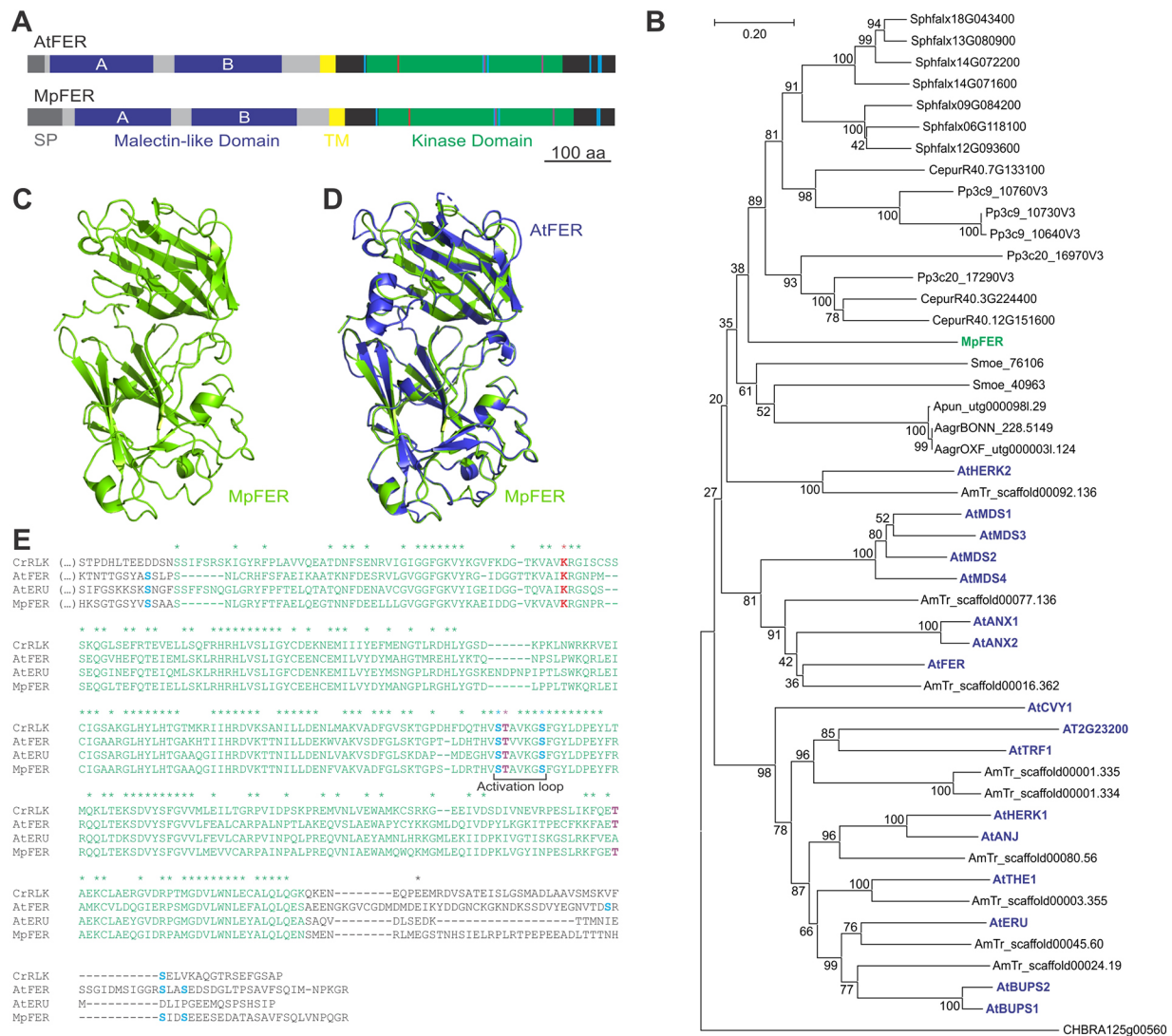


Fig. 1. CrRLK1Ls are conserved among land plants. (A) Representation of AtFER and MpFER proteins. The malectin domains are represented in blue and kinase domains in green. SP, signal peptide; TM, transmembrane domain (yellow). Amino acids important for regulation and activity are marked in red, violet and light blue as described in E. (B) A rooted neighbor-joining tree of the amino acid sequence of the predicted malectin-like domain (corresponding to aa 76–431 of MpFER). *CrRLK1L* members from *Marchantia polymorpha* (Mp, green), *Physcomitrium patens* (Pp), *Sphagnum fallax* (Sphfalx), *Ceratodon purpureus* (Cepur), *Anthoceros agrestis* Bonn (AagrBONN), *Anthoceros agrestis* Oxford (AagrOXR), *Anthoceros punctatus* (Apun), *Selaginella moellendorffii* (Smoe), *Amborella trichopoda* (AmTr) and *Arabidopsis thaliana* (At, blue) were used. The best hit from *Chara braunii* (CHBRA) was also included. The numbers indicate the bootstrap values (%) from 1000 replications. The given scale represents a substitution frequency of 0.1 amino acids per site. (C) Schematics of the predicted 3D structure of the MpFER malectin-like domain, showing predicted α -helix and β -sheet structures. (D) Structural superposition of the malectin-like domains of AtFER (blue) and MpFER (green). (E) Alignment of the cytoplasmic domains of MpFER, AtERU, AtFER and CrRLK1 (CrRLK). Kinase domains are in green, putative phosphorylation sites in light blue (Ser) and violet (Thr), and the conserved catalytic Lys in red. See also Fig. S1.

α -helices (Fig. 1C). When comparing the structural superposition of the AtFER and MpFER ECDs (Fig. 1D, Fig. S1D), we observed that most conserved parts of the malectin-like domain are in the core of the protein, and the more variable parts are located peripherally. Moreover, the 3D structure of the CpRLK1 ECD could not be properly modeled using the AtFER ECD (Fig. S1D,E), and neither could that of *C. braunii* (Fig. S1D,F). Taken together, these results suggest that the malectin-like domain of MpFER could interact with similar proteins as AtFER does in *A. thaliana* and may thus be involved in similar pathways. Sequence comparison of the MpFER kinase domain showed conservation of the activation loop and a Lys residue important for catalytic activity (Fig. 1E). Furthermore, several determined phosphorylation sites found in AtFER, AtERU and CrRLK1 were conserved in MpFER (Fig. 1E) (Schoenaers

et al., 2018; Haruta et al., 2014; Liu et al., 2016; Schulze-Muth et al., 1996). Given that the genomes of *M. polymorpha* and *Anthoceros* spp. encode a single CrRLK1L and this RK family is not present in Charophycean algae, we propose MpFER to be basal and orthologous to all other land plant CrRLK1Ls, and that the CrRLK1L family arose as plants conquered land.

MpFER is broadly expressed throughout the *M. polymorpha* life cycle

In *A. thaliana*, the expression patterns of the 17 CrRLK1L members span vegetative and reproductive stages and both generations of the life cycle (reviewed by Lindner et al., 2012), pointing to the importance of CrRLK1Ls for basic cellular functions. To assess whether this pattern is reflected in the land plant with the most

ancestral characteristics, a promoter fragment of 3.2 kb (*proMpFER*) was used to drive expression of a triple yellow fluorescent protein (*trpVNS*) with a nuclear localization signal (*proMpFER:trpVNS*) and transformed into *M. polymorpha* sporelings. All transformants expressing the *trpVNS* fluorescent protein (45 of 48 independent lines) exhibited an indistinguishable expression pattern (Fig. 2). During vegetative stages of gametophyte development, expression was observed in most cells of the thallus (Fig. 2A,B). In concordance with the importance of *MpFER* for rhizoids (Honkanen et al., 2016), high *trpVNS* expression was observed in these tip-growing cells (Fig. 2A',B'). Although *trpVNS* was expressed in gemma cups, no expression was observed in mature gemmae (clonal, asexual propagules produced in the gemma cups), possibly owing to their dormancy (Fig. 2C,D).

In mature female sexual organs, strong expression was observed in the entire archegoniophore (Fig. 2E,F). The archegonia expressed *trpVNS* in most cells, except for the egg cell (Fig. 2G). However, after fertilization, *proMpFER:trpVNS* became active in the zygote (Fig. 2H). In male sexual organs, *trpVNS* was broadly detected in the antheridial splash platform (Fig. 2I,J) and, specifically, in the spermatogenous tissue of the antheridia and the non-reproductive jacket cells surrounding them at different developmental stages (Fig. 2K). Inside the sporogonium, the sporogenous cells, and subsequently the developing spores, but not the elater cells, strongly expressed *trpVNS* (Fig. 2L).

Taken together, *MpFER* is expressed in most tissues during the vegetative stages of gametophyte development as well as in the antheridia and archegonia during sexual reproduction. Interestingly, the *proMpFER* promoter was not active in mature gemmae and the unfertilized, quiescent egg cell, although expression was initiated

after dormancy and in the zygote. In concordance with the collectively ubiquitous expression of *CrRLK1Ls* in *A. thaliana*, the *MpFER* expression pattern reinforces the importance of this family for basic cellular functions in land plants.

MpFER controls cell expansion during vegetative gametophyte development

To analyze the function of *MpFER*, three independent artificial microRNA constructs targeting *MpFER* were designed (*amiR-MpFER*), based on the endogenous microRNA *MpmiR160* (Fig. S2; Flores-Sandoval et al., 2016) and driven by the ubiquitous *proMpEF1* promoter (Althoff et al., 2014). Whereas *amiR-MpFER1* and *amiR-MpFER2* target sites in the ECD coding sequence, *amiR-MpFER3* targets the sequence encoding the kinase domain (Fig. 3A,B). For each *amiR-MpFER* construct, several independent transgenic lines were obtained that showed a reduction in thallus size (Fig. 3C,D, Fig. S3A). *MpFER* levels were quantified by quantitative reverse transcription PCR (qRT-PCR) in two independent *amiR-MpFER2* and *amiR-MpFER3* lines each, which showed a similar phenotype (Fig. 3E). *MpFER* expression ranged from 10% to 20% of the wild-type level in all *amiR-MpFER* lines analyzed (Fig. 3E).

Previously, the T-DNA insertion mutant *Mpfer-1* was identified in a screen for mutants with defective rhizoids (Honkanen et al., 2016; referred to as *Mpthe*). As the T-DNA inserted into the 3' UTR of the *MpFER* gene (Fig. 3A; Honkanen et al., 2016), *MpFER* expression was analyzed by qRT-PCR, but it showed no reduction compared with the wild type (Fig. S3B), suggesting that the T-DNA insertion does not affect *MpFER* transcription. Sequencing of the *MpFER* coding sequence in the *Mpfer-1* mutant did not show any

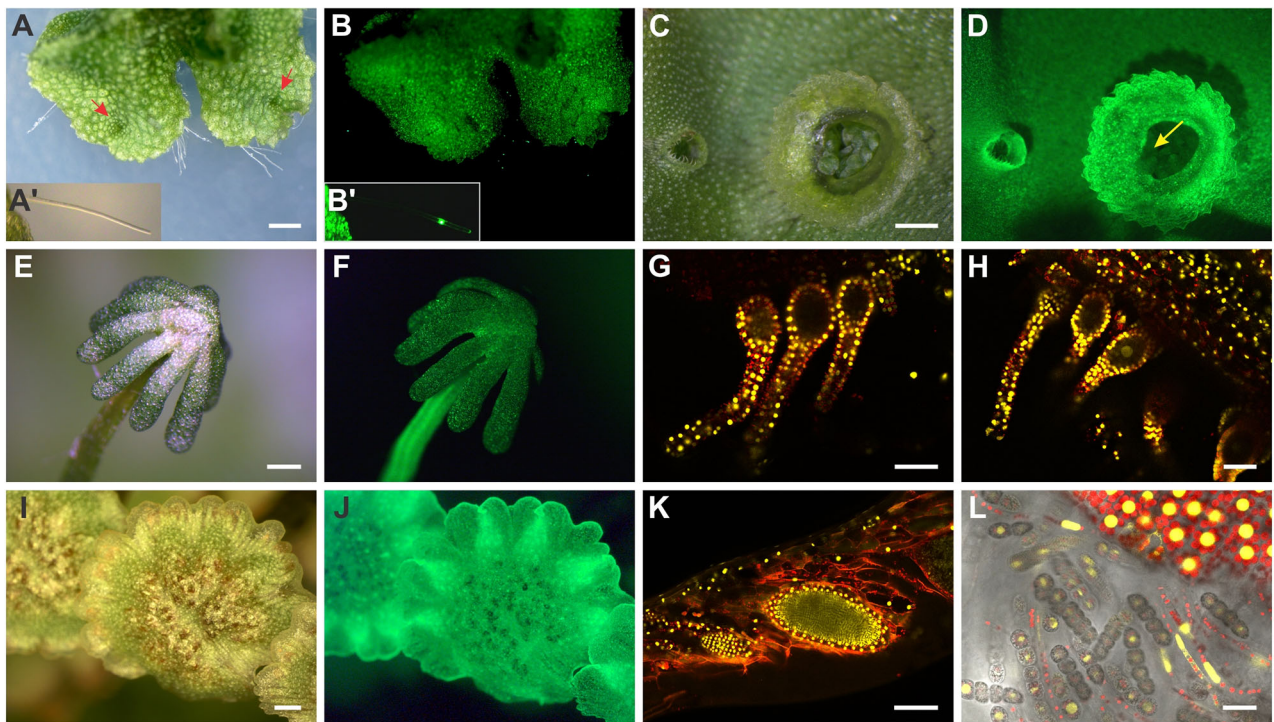


Fig. 2. *MpFER* is broadly expressed in most tissues throughout the *M. polymorpha* life cycle. (A–L) Expression of *proMpFER:trpVNS* in different organs of male and female *M. polymorpha* plants. Fluorescence is visualized as either green (epifluorescence microscope) or yellow (confocal microscope), depending on the panel. (A–F) Brightfield (A,C,E) and epifluorescence (B,D,F) images of a thallus (A,B), rhizoid (A',B'), gemmae cups (C,D) and an archegoniophore (E,F). Red arrows indicate meristematic zones, the yellow arrow a gemma. Scale bars: 0.5 mm. (G,H) Confocal images of archegonia before (G) and 2 days after (H) fertilization. Scale bar: 50 μ m. (I,J) Brightfield (I) and epifluorescence (J) images of an antheridiophore. Scale bar: 1 mm. (K) Confocal image of antheridia. Scale bar: 100 μ m. (L) Confocal image of sporophyte and spores. Scale bar: 25 μ m.

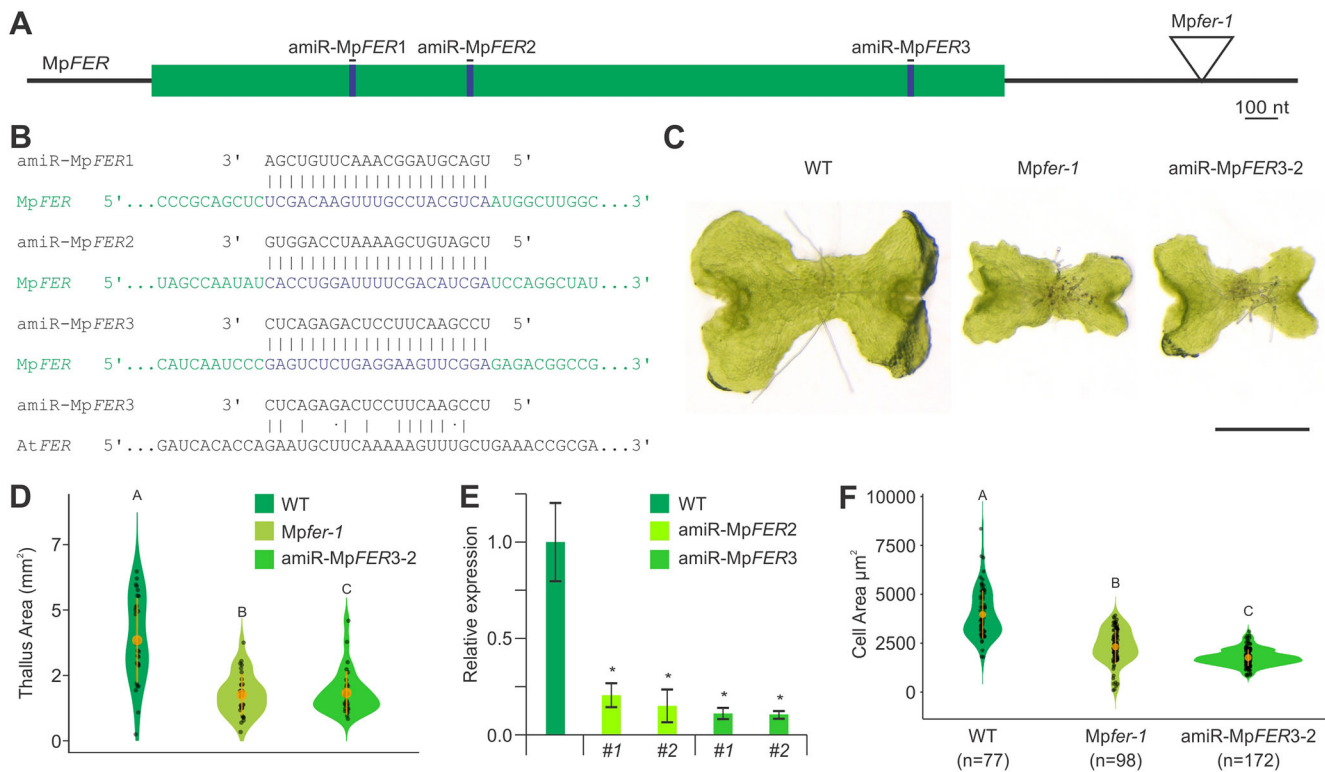


Fig. 3. *MpFER* controls cell size during gametophyte development. (A) Representation of the mature *MpFER* mRNA. The coding sequence is in green, locations of the amiRNA target sites in blue. The location of the T-DNA insertion in *Mpfer-1* is shown. (B) Base complementary of mature amiR-*MpFER1*, amiR-*MpFER2* and amiR-*MpFER3* with the *MpFER* transcript. Very low complementarity was found between amiR-*MpFER3* and *AtFER*. (C) Representative pictures of 10-day-old gemmalings of wild-type (WT), *Mpfer-1* and amiR-*MpFER3-2* lines. Scale bar: 1 mm. (D) Violin plot of thallus area of 14-day-old gemmalings of WT, *Mpfer-1* and amiR-*MpFER3-2* lines. $n=30$. Different letters indicate significant differences according to the non-parametric Kruskal–Wallis test and Dunn’s test for multiple comparisons ($P<0.001$). Orange circles indicate the group mean and the corresponding vertical bars the standard deviation for each group. (E) Relative expression level of *MpFER* in thallus tissue from WT and two independent insertion lines of amiR-*MpFER2* and amiR-*MpFER3*, as measured by qRT-PCR. *MpEF1* was used as internal control. Shown are mean \pm s.e.m. of three biological replicates. Statistical analysis was performed by one-way analysis of variance (ANOVA) followed by a post-hoc Duncan test ($*P<0.01$). (F) Violin plot of cell size in WT, *Mpfer-1* and amiR-*MpFER3-2* lines. Only areas with fully expanded cells in approximately 3-week-old plants were used for measurements. Different letters indicate significant differences according to the non-parametric Kruskal–Wallis test and Dunn’s test for multiple comparisons ($P<0.001$). Orange circles indicate the group mean and the corresponding vertical bars the standard deviation for each group. See also Figs S2 and S3.

mutation, and 3’ RACE-PCR showed that transcript terminated about 1.3 kb inside the T-DNA and was not polyadenylated (Fig. S3C). Because the thallus size of *Mpfer-1* mutants is similar to that of amiR-*MpFER* lines (Fig. 3C,D, Fig. S3A) and efficient translation depends on the presence of a poly(A)-tail (Sachs and Varani, 2000), we propose that *MpFER* protein levels are reduced in the *Mpfer-1* mutant despite normal transcript levels.

Rhizoids are tip-growing cells analogous to the root hairs of flowering plants (angiosperms). Reduced *MpFER* activity strongly impaired rhizoid formation and the rhizoids collapsed (Fig. S3D). This had also been reported for the *Mpfer-1* mutant (Honkanen et al., 2016) and is in concordance with the function of *AtFER* and *AtANX1/2* in tip-growing root hairs (Bai et al., 2014; Duan et al., 2010; Haruta et al., 2014; Gonneau et al., 2018) and pollen tubes (Boisson-Dernier et al., 2009; Miyazaki et al., 2009), respectively. As *CrRLK1L* members are important for cell expansion in angiosperms (Hématy et al., 2007; Guo et al., 2009a; Kessler et al., 2010; Li et al., 2015; Dünser et al., 2019; Gachomo et al., 2014; Merz et al., 2017), the size of epidermal thallus cells in fully differentiated regions with minimal growth was measured in *Mpfer-1* and amiR-*MpFER* lines, showing a reduction in cell area compared with the wild type (Fig. 3F, Fig. S3E,F). The average epidermal cell area was similarly reduced, although the distribution of cell areas differed between amiR-*MpFER* lines and *Mpfer-1* (Fig. 3F, Fig. S3E,F).

In conclusion, *MpFER* has a fundamental role in rhizoid formation and cellular growth during vegetative development. These results suggest an ancestral and conserved function of the *CrRLK1L*s in polar tip growth and cell expansion.

***MpFER* is important for the morphological integrity of the gametophyte**

Given that *Mpfer-1* and amiR-*MpFER* lines retain some *MpFER* activity, we generated *Mpfer* knockout mutants with the goal of unveiling potentially hidden *CrRLK1L* functions by generating a plant without any *CrRLK1L* activity. Using CRISPR/Cas9, two sites in the ECD-coding sequence of *MpFER* were targeted (Fig. 4A,B). At least ten independent lines were selected and analyzed for each target site. All plants with severely affected thallus development contained a frame-shift mutation at the respective target site (Fig. 4B,C) but *MpFER* was not affected in transgenic plants with normal development.

The thallus area of the newly generated, amorphic knockout mutants was more strongly reduced compared with *Mpfer-1* (Honkanen et al., 2016), confirming that, like the amiR-*MpFER* lines, *Mpfer-1* is a hypomorphic mutant (Fig. 4C,D). In contrast, rhizoid integrity was similarly affected in hypo- and amorphic *Mpfer* alleles, suggesting that rhizoid formation is more sensitive to reduced *MpFER* activity than is thallus growth (Fig. 4E,F). Despite

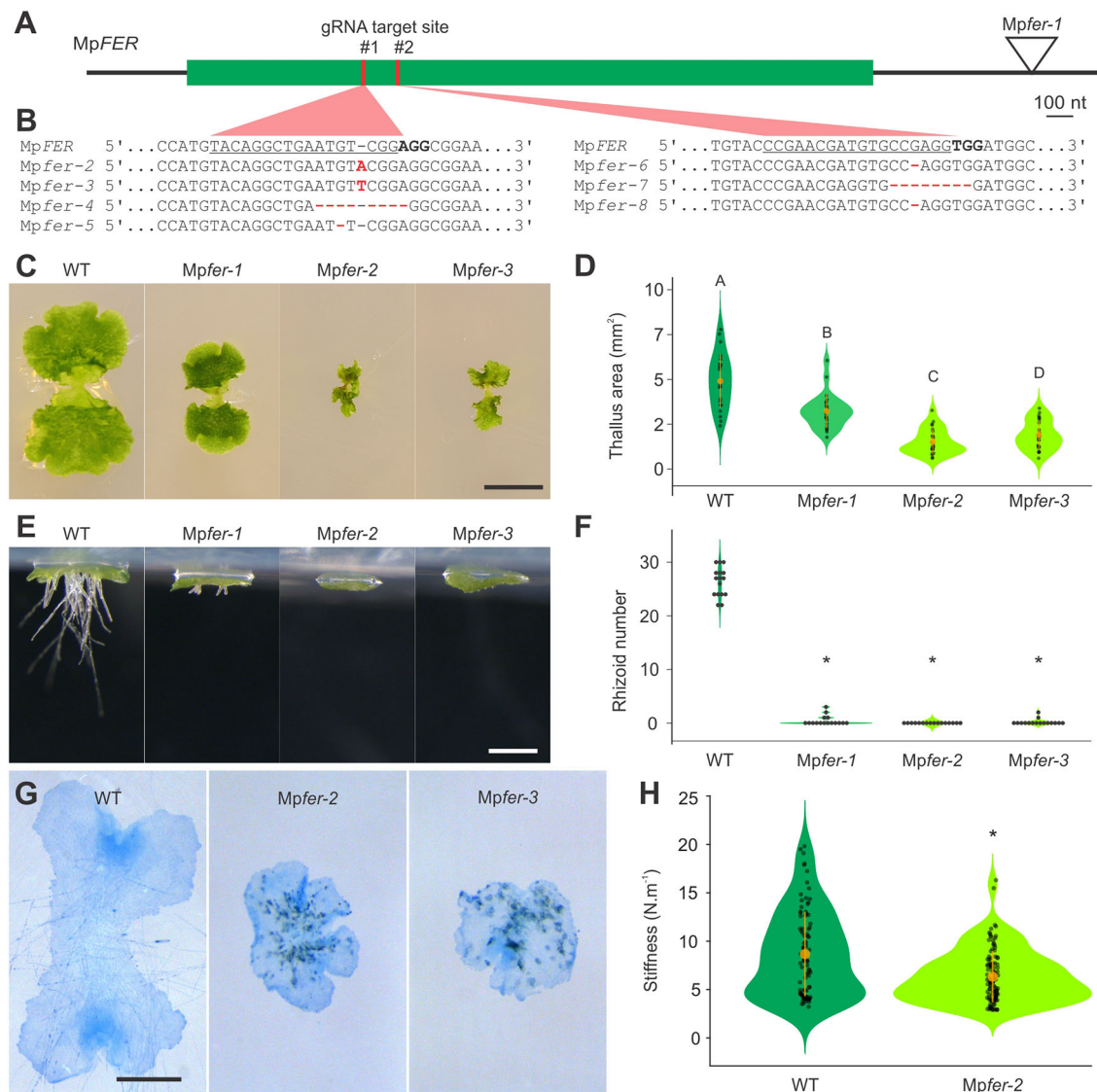


Fig. 4. The integrity of thalli from *Mpfer* knockout lines is severely affected. (A) Representation of the mature *MpFER* mRNA with the coding sequence in green, and the location of the gRNA target sites in red. (B) Sequences of gRNA target sites in the confirmed *Mpfer* knockout mutants. Deletions and insertions are highlighted in red. (C) Representative pictures of 14-day-old gemmalings of the wild type (WT), *Mpfer-1* and two independent *Mpfer* knockout mutants. Scale bar: 0.5 cm. (D) Violin plot of thallus area of 7-day-old gemmalings of WT, *Mpfer-1* and two independent *Mpfer* knockout mutants. $n=25$. Different letters indicate significant differences in a one-way analysis of variance (ANOVA) followed by a post-hoc Duncan test ($P<0.01$). Orange circles indicate the group mean and the corresponding vertical bars the standard deviation for each group. (E) Representative pictures of 7-day-old gemmalings growing in upside-down plates of WT, *Mpfer-1* and two independent *Mpfer* knock-out mutants. Scale bar: 500 μm . (F) Violin plot of rhizoid number in 3-day-old gemmalings of WT, *Mpfer-1* and two independent *Mpfer* knockout mutants. $n=16$. Statistical analysis was performed by one-way analysis of variance (ANOVA) followed by a post-hoc Duncan test ($*P<0.01$). (G) Trypan Blue staining of 7-day-old gemmalings of WT, *Mpfer-1* and two independent *Mpfer* knockout mutants. Scale bar: 1 mm. (H) Violin plot of the reduction in the apparent stiffness of gemmaling tissue in *Mpfer-2* compared with the WT. Statistical analysis was performed using a Kruskal–Wallis test followed by a Tukey–Kramer post-hoc test ($*P<0.001$). Orange circles indicate the group mean and the corresponding vertical bars the standard deviation for each group.

the strong impact on thallus development, both hypo- and amorphic *Mpfer* mutants form gemma cups.

The strong disruption of thallus growth in amorphic *Mpfer* mutants prompted us to investigate whether cells of the thallus died in the absence of *MpFER* activity. Indeed, using Trypan Blue staining, we detected dead cells in these mutants, indicating a loss of morphological integrity (Fig. 4G). To investigate the mechanical properties of thallus cells, we measured their apparent stiffness using cellular force microscopy on 3-day-old gemmalings (plantlets derived from a gemma) and found that amorphic *Mpfer-2* mutants had a lower apparent stiffness than the wild type (Fig. 4H).

The apparent stiffness of the thalli depends on both the stiffness of the cell wall and the turgor pressure of the cells. Because the apparent stiffness is lower in *Mpfer-2* mutants, it is likely that a reduction in the stiffness of their cell wall causes the cells to burst and die.

Some reproductive but not all CWI-sensing functions of *CrRLK1Ls* are conserved in land plants

In *A. thaliana*, at least seven *CrRLK1L* family members play a role in reproduction, with *AtANX1/2* and *AtBUPS1/2* being important for pollen tube growth (Boisson-Dernier et al., 2009; Miyazaki

et al., 2009; Zhu et al., 2018; Ge et al., 2017) and *AtFER*, *AtHERK1* and *AtANJ* for pollen tube reception by the synergid cells (Escobar-Restrepo et al., 2007; Galindo-Trigo et al., 2020). To characterize the function of *MpFER* in reproductive development, amiR-*MpFER3* lines were transferred to sexual organ-inducing conditions (Chiyoda et al., 2008). The number of antheridiophores

produced was significantly lower in amiR-*MpFER* lines compared with the wild type (Fig. 5A, Fig. S3G) and the antheridiophore splash platforms were also smaller (Fig. 5B). The reduction in *MpFER* expression in antheridiophores of amiR-*MpFER* lines was confirmed by qRT-PCR and results were comparable to those using thallus tissue (Fig. 5C). A pronounced reduction in spermatogenous

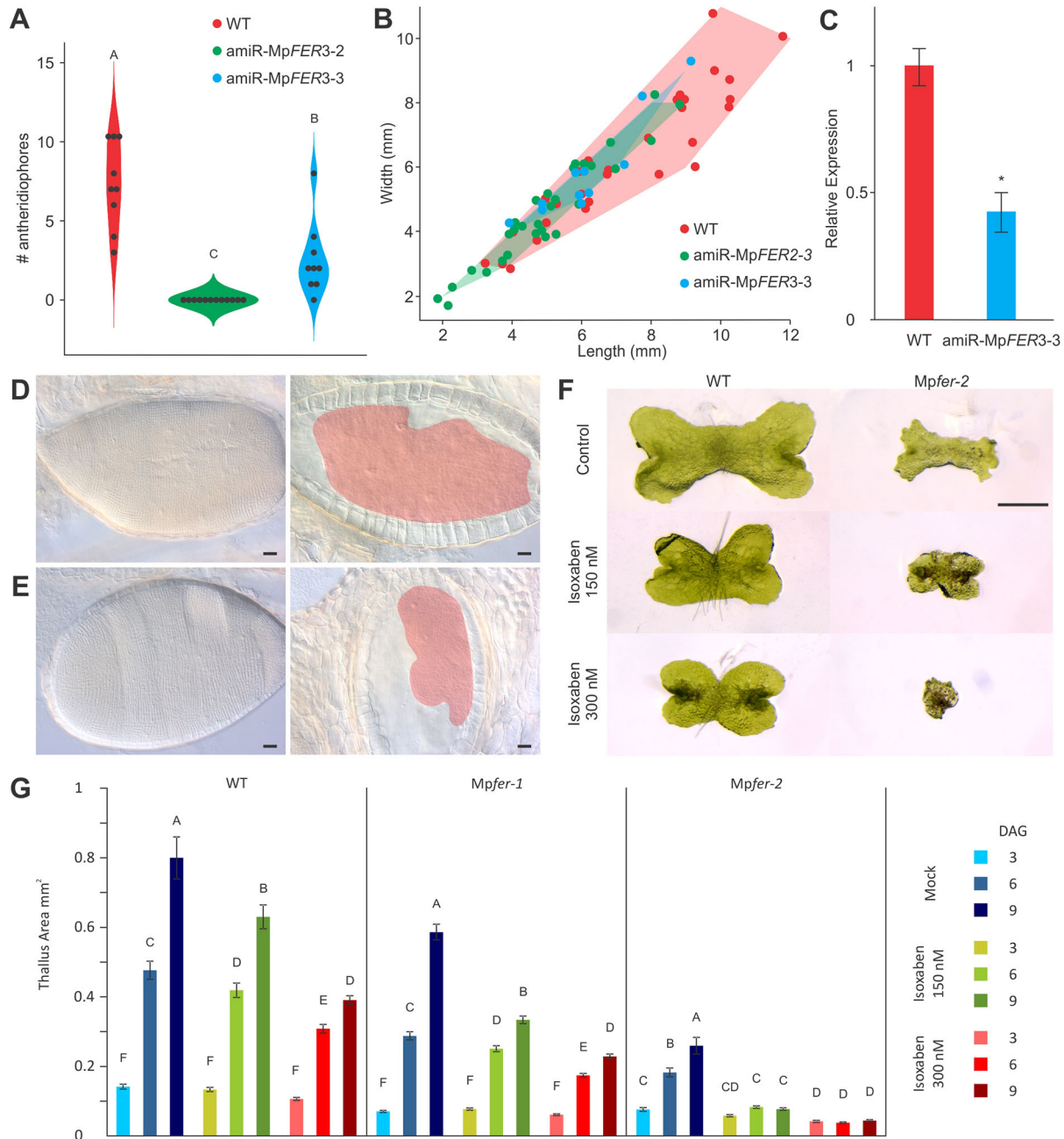


Fig. 5. Conservation of *CrRLK1L* function in land plants. (A) Violin plot of the number of antheridiophores produced per plant for wild type (WT, $n=9$) and two independent amiR-*MpFER3* lines (amiR-*MpFER3-2*, $n=9$; amiR-*MpFER3-3*, $n=12$). Different letters indicate a significant difference in a one-way analysis of variance (ANOVA) followed by a post-hoc Duncan test ($P<0.01$). (B) Antheridiophore splash platform size distribution of WT ($n=32$), amiR-*MpFER2-3* ($n=34$) and amiR-*MpFER3-3* ($n=11$) lines. For all antheridia with a stalk >8 mm, length and width of the platform were recorded. Shaded areas represent the range of data points, illustrating the larger variation of splash platform size in the WT. (C) qRT-PCR of *MpFER* levels in antheridiophores in a WT and amiR-*MpFER3-3* line. *MpEF1* was used as internal control. Shown are mean \pm s.e.m. of three biological replicates. Statistical analysis was performed by one-way analysis of variance (ANOVA) followed by a post-hoc Duncan test ($*P<0.01$). (D,E) Brightfield images (left) and optical cross-sections (right) of mature antheridia of a WT (D) and amiR-*MpFER3-3* line (E). The spermatogenous areas are shaded in red. Scale bars: 100 μ m. (F) Representative pictures of 6-day-old gemmalings of WT and *Mpfer-2* mutants at different isoxaben concentrations. Scale bar: 1 mm. (G) Thallus area of gemmalings of WT, *Mpfer-1* and *Mpfer-2* lines growing on media containing different isoxaben concentrations. $n=35$. Data are mean \pm s.e.m. of two biological replicates. Different letters indicate a significant difference in a one-way analysis of variance (ANOVA) followed by a post-hoc Duncan test ($P<0.05$). DAG, days after gemmae-planting. See also Fig. S3.

tissue was observed in many antheridia isolated from amiR-MpFER3-3 lines (Fig. 5D,E). Whether this phenotype is caused by reduced cell expansion, as was observed in thalli, or by a lower cell division rate is currently unclear. Moreover, although the plants were grown under optimal conditions in axenic culture boxes, the effects on reproductive structures could be partly indirect and due to the reduction in plant size and/or rhizoid function.

To determine male fertility of these amiR-MpFER lines with reduced spermatogenous tissue, we performed crosses with wild-type female plants. The spermatocyte concentration harvested from wild-type antheridia was almost threefold higher than from amiR-MpFER lines and was adjusted using a hemocytometer. In just one of the crosses ($n=20$), a single sporophyte was formed, resulting in 0.05 ± 0.05 (mean \pm s.e.m.) sporophytes per archegoniophore, whereas the same females crossed with wild-type males yielded 9.95 ± 2.33 (mean \pm s.e.m.) sporophytes per archegoniophore. In summary, MpFER plays a role in antheridiophore development, and spermatocytes of plants with reduced MpFER activity are poorly fertile. Thus, CrRLK1Ls have a conserved role in reproduction in addition to their role in cell expansion and integrity during vegetative development.

Some *A. thaliana* CrRLK1Ls are involved in surveying CWI and in inhibiting growth when CWI is impaired. Cell wall defects caused either by mutations affecting cellulose biosynthesis or by treatment with isoxaben, a cellulose synthesis inhibitor, can be suppressed by a mutation in *AtTHE1* (Hématy et al., 2007; Denness et al., 2011). To investigate whether MpFER also acts as CWI sensor, we treated wild-type, *Mpfer-1* and *Mpfer-2* gemmae with isoxaben (Fig. 5F,G). As in the wild type, isoxaben affected the development of gemmae with reduced MpFER activity, all growing progressively less with increasing isoxaben concentration (Fig. 5F,G). Moreover, isoxaben treatment was lethal for *Mpfer-2* knockout mutants (Fig. 5F,G). Similar observations were reported for *Atfer-4*, where isoxaben treatment increased the number of dead cells in hypocotyls (Malivert et al., 2021). These results suggest that the function of *AtTHE1* in repressing cellular growth when CWI is impaired appeared later in the course of land plant evolution or was lost in the *Marchantia* lineage.

The CrRLK1L signaling pathway is conserved in land plants

As downregulation of MpFER or AtFER produce similar phenotypes concerning polarized growth and cell expansion in *M. polymorpha* and *A. thaliana*, respectively, interspecific complementation was attempted. First, the coding sequence of MpFER fused to the Green Fluorescent Protein (GFP) gene under the control of the viral 35S promoter ($_{pro}35S:MpFER-GFP$) was transformed into heterozygous *Atfer-1* mutants. Then, GFP expression at the cell periphery and complementation of the bursting root hair and reduced rosette size phenotypes were assessed in transgenic plants (Fig. 6A). *Atfer-1* homozygotes expressing the MpFER-GFP protein look similar to *Atfer-1* mutants, indicating that MpFER does not complement these *Atfer-1* loss-of-function phenotypes (Fig. 6A). Although we cannot exclude the possibility that this is because we used a heterologous promoter, we consider this unlikely as expression the 35S promoter is routinely used to complement root hair phenotypes (Baumberger et al., 2001; Kim and Dolan, 2016). In a complementary experiment, the coding sequence of AtFER fused to the Citrine gene under the control of the MpEF1 promoter ($_{pro}MpEF1:AtFER-Cit$) was transformed into amiR-MpFER3-2 plants. Ten independent lines with Citrine expression at the cell periphery were phenotypically characterized (Fig. 6B,C). All had bursting rhizoids and a reduced thallus size,

similar to the parental amiR-MpFER3-2 line, suggesting that AtFER does not rescue the vegetative phenotypes produced by downregulation of MpFER. A sequence alignment of AtFER with amiR-MpFER3 showed no complementarity (Fig. 3B), confirming that the failure to complement is not caused by a potential downregulation of AtFER by amiR-MpFER3. Taken together, these results show that MpFER and AtFER cannot substitute for each other with respect to their function in cell expansion and tip growth.

In *A. thaliana*, it was shown that AtFER forms a complex with AtRALF peptides and the LRE/LLG co-receptors (Xiao et al., 2019). As no interspecific complementation was observed, the conservation of binding surfaces between CrRLK1L, RALF and LRE homologs were analyzed. The *M. polymorpha* genome encodes three RALF peptides [MpRALF: Mp1g27120 (Mapoly0002s0166); MpRALF2: Mp2g21670 (Mapoly0040s0047); MpRALF3: Mp7g07270 (Mapoly0076s0067)] (Galindo-Trigo et al., 2016; Bowman et al., 2017). We performed phylogenetic analysis using the amino acid sequences of the predicted mature peptides of *A. thaliana* and *M. polymorpha* RALFs (Fig. S4A). All MpRALF peptides clustered together with AtRALFs known to interact with CrRLK1L receptors, including AtRALF1 and AtRALF23, which serve as AtFER ligands (Stegmann et al., 2017; Haruta et al., 2014) (Fig. S4A). The MpRALFs shared the four conserved Cys residues as well as the YXXY and YY motifs with the AtRALF1 subgroup (Fig. S4B). However, only MpRALF1 and MpRALF3 had an RRXL motif, which is important for cleavage by the S1P protease (Fig. S4B,C) (Srivastava et al., 2009), consistent with the presence of one S1P ortholog in basal plants [Mp8g07990 (Mapoly0155s0018); Fig. S4D]. There are two MpLRE/LLG proteins encoded in the *M. polymorpha* genome (Fig. S5A,B). Both the MpLRE1 [Mp5g09600 (Mapoly0048s0110)] and MpLRE2 [Mp4g22100 (Mapoly0090s0020)] proteins showed conservation of the eight Cys residues and the ND motif characteristic of the family (Fig. S5B); however, MpLRE1 did not contain a GPI-anchoring site (Fig. S5B). Structure prediction using AtLLG1 as a template (Xiao et al., 2019) showed a conserved general structure (Fig. S5C,D). Some of the MpRALF and MpLRE family members showed a similar expression pattern as MpFER (Fig. S5F), suggesting that the corresponding proteins could form a complex similar to that described in *A. thaliana*.

To gain insights into the formation of a putative CrRLK1L signaling complex, the MpFER/MpRALF/MpLRE complex was modeled. The general structure appeared to be conserved (Fig. S5E); however, analysis of conserved sites between *M. polymorpha* and *A. thaliana* showed a low amino acid conservation in the interacting surfaces of the complex subunits (Fig. 6D). This suggests that the lack of interspecific complementation may be due to differences in amino acids that are important for complex formation, and that the proteins forming the complex have diverged, following distinct routes of co-evolution in the two lineages.

Because interspecific complementation of the amiR-MpFER phenotypes was unsuccessful, we investigated whether suppression using a downstream component of CrRLK1L signaling identified in *A. thaliana* was possible. AtMRI, a receptor-like cytoplasmic kinase, acts downstream of AtFER or AtANXI/2 in the regulation of polar tip growth (Boisson-Dernier et al., 2015; Liao et al., 2016). The dominant AtMRI^{R240C} mutation can suppress pollen tube rupture in the *Atanx1 Atanx2* double mutant and the root hair defects of *Atfer-4* (Boisson-Dernier et al., 2015; Liao et al., 2016). A mutation in MpMRI (also known as MpPTI), with a bursting rhizoid phenotype similar to that observed in *Mpfer-1*, was

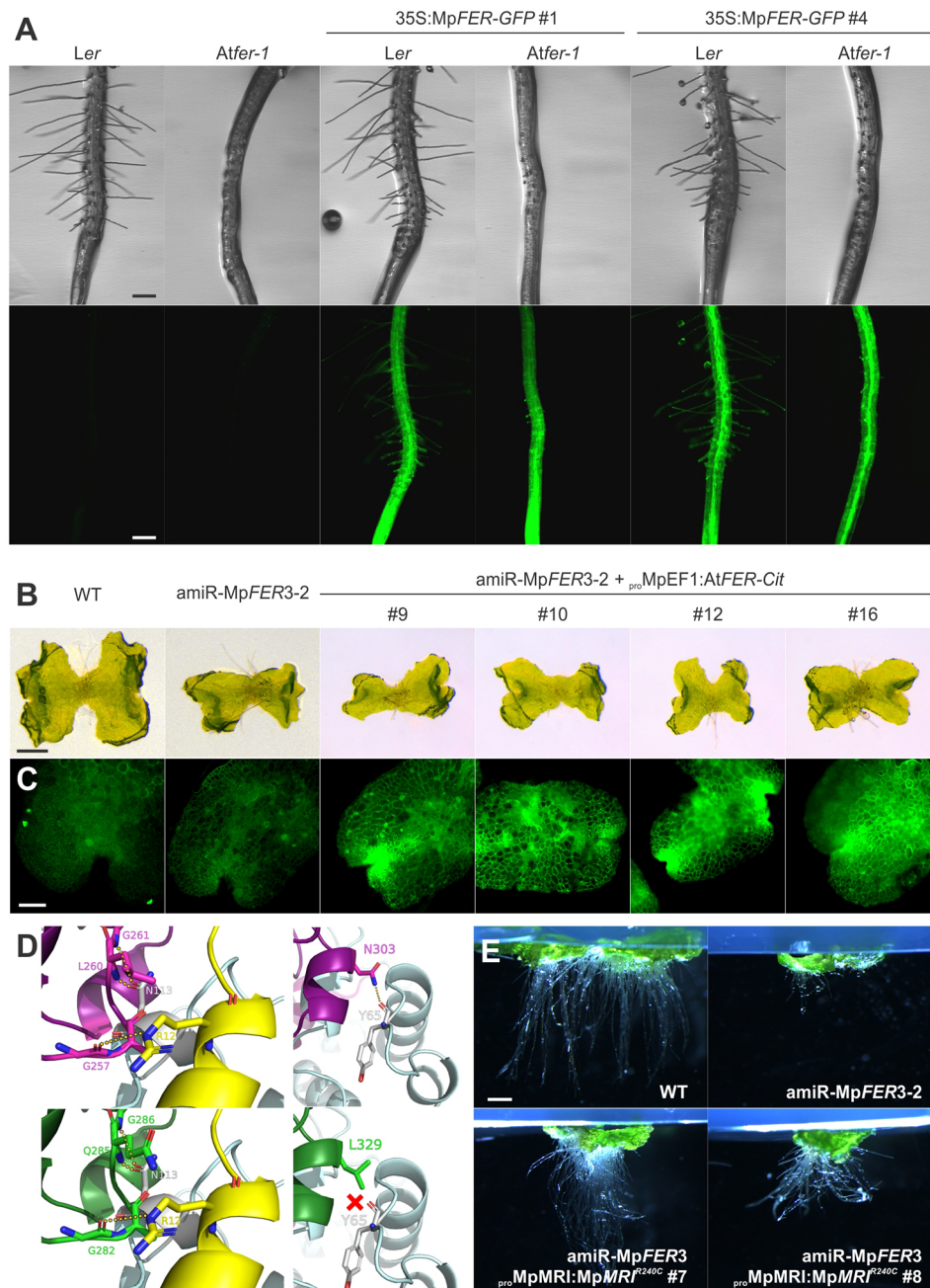


Fig. 6. Interspecific complementation of *A. thaliana* and *M. polymorpha* plants with reduced levels of *FER* activity.

(A) Bright-field (upper row) and epifluorescence (lower row) pictures of roots of independent *A. thaliana* lines expressing *pro*-35S:MpFER-GFP in *Ler* wild-type (WT) and *Atfer-1* plants. Scale bars: 200 μ m. (B) Ten-day-old gemmalings of WT and amiR-MpFER3-2 *M. polymorpha* plants with and without expression of *AtFER-Cit*. Scale bar: 0.5 mm. (C) Citrine expression in 7-day-old gemmalings of WT and amiR-MpFER3-2 plants with and without expression of *AtFER-Cit*. Scale bar: 100 μ m. (D) Schematics of the CrRLK1L^{ECD} polar interactions sites with LRE/RALF when forming a protein complex. Upper panels correspond to contact areas between *AtFER* (purple), *AtLLG2* (blue-gray) and *AtRALF23* (yellow), and lower panels to the modeled MpFER structure (green) superimposed onto the same complex. Polar interactions are depicted as dotted yellow lines. Left panels show the predicted polar interactions of the complex that are conserved between *A. thaliana* and *M. polymorpha*, whereas the right panels show the polar interaction between *AtFER* and *AtLLG2* that is predicted to be absent between MpFER and *AtLLG2*. (E) Suppression of the amiR-MpFER3-2 phenotype by a dominant-active version of MpMRI under its own promoter (*pro*MpMRI:MpMRI^{R240C}). In addition to the WT and amiR-MpFER3-2 controls, two independent *pro*MpMRI:MpMRI^{R240C} lines with partial suppression of the rhizoid phenotype are shown. Scale bar: 1 mm. See also Figs S4-S6.

identified in the same genetic screen for *M. polymorpha* mutants with defective rhizoids (Honkanen et al., 2016). To test whether MpMRI is a conserved downstream component of the MpFER signal transduction pathway, a dominant-active form of the protein equivalent to *AtMRI*^{R240C} was transformed into the amiR-MpFER3-2 line, driven by 2 kb of the endogenous promoter (*pro*MpMRI:MpMRI^{R240C}). Several independent lines showed a partial restoration of rhizoid growth; however, we also observed defects in thallus development of lines with higher levels of MpMRI expression, mainly abnormalities in the epidermis (Fig. 6E, Fig. S6A-E). This suggests that MpMRI acts downstream of MpFER in the signal transduction pathway controlling polarized growth since the origin of land plants, in agreement with a recent report on the functional characterization of MpMRI (Westermann et al., 2019).

Overexpression of MpFER affects morphological integrity

Because overexpressing *AtFER* in *M. polymorpha* did not lead to any obvious phenotypes or complementation of amiR-MpFER lines (Fig. 6B,C), we also overexpressed *AtFER* and MpFER in the wild type. As in the amiR-MpFER background, overexpression of *AtFER* (*pro*MpEF1:*AtFER-Cit*) in a wild-type background had no effect, consistent with the idea that *AtFER* is unable to form a complex with the corresponding *M. polymorpha* proteins. However, when expressing an MpFER-Citrine fusion protein (*pro*MpEF1:MpFER-Cit) in wild-type plants, thallus development was strongly affected (Fig. 7A). As expected, MpFER-Cit localized to the membrane (Fig. 7A, inset), and higher protein levels correlated with a more severe phenotype (Fig. S6F,G). Scanning electron microscopy of the epidermis of plants expressing high levels of MpFER showed defects in the formation of air chambers and air

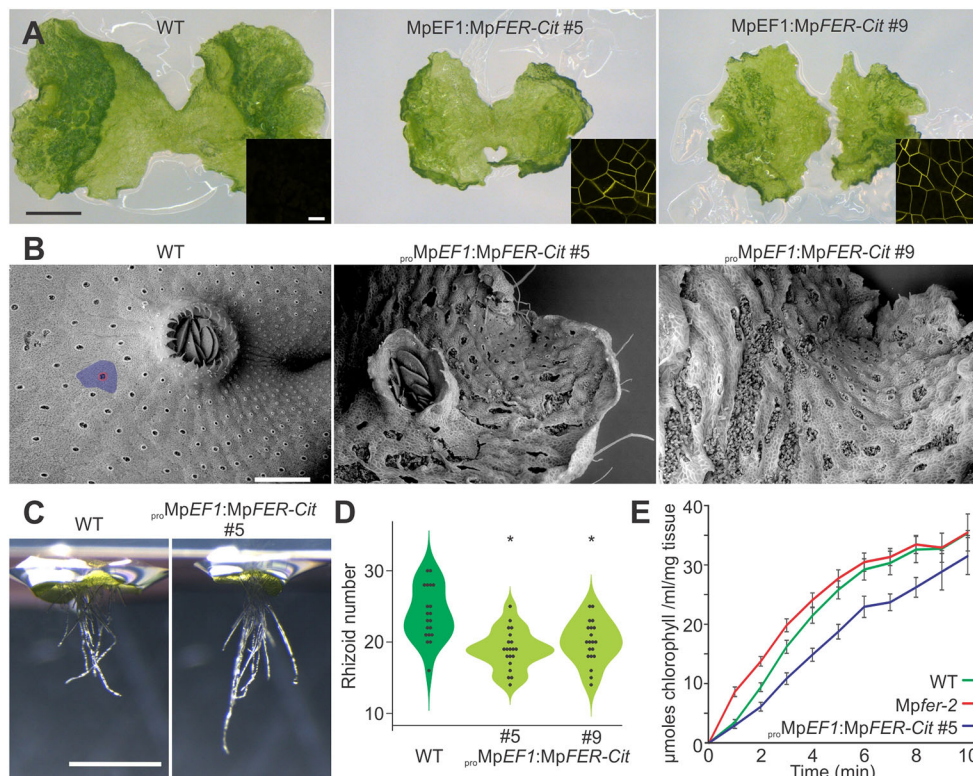


Fig. 7. Overexpression of MpFER affects morphological integrity.

(A) Representative pictures of 10-day-old gemmalings of wild type (WT) and two different lines overexpressing MpFER (*proMpEF1:MpFER-Cit*). Scale bar: 1 mm. Insets show Citrine expression at the plasma membrane in *proMpEF1:MpFER-Cit* lines #5 and #9 as observed by confocal microscopy. Scale bar: 20 μ m. (B) Scanning electron microscopical images of thalli from 20-day-old plants of WT and *proMpEF1:MpFER-Cit* lines #5 and #9. The blue region demarks an air chamber, and air pore cells are colored in red. Scale bar: 500 μ m. (C) Representative pictures of 3-day-old gemmalings growing in upside-down plates of WT and *proMpEF1:MpFER-Cit* #5 lines. Scale bar: 1 mm. (D) Violin plot of the number of rhizoids in 3-day-old gemmalings of WT and *proMpEF1:MpFER-Cit* lines #5 and #9. $n=20$. Statistical analysis was performed by one-way analysis of variance (ANOVA) followed by a post-hoc Duncan test ($*P<0.01$). (E) Graphs showing the amount of effluxed chlorophyll as a function of time from 15-day-old gemmalings of WT, *Mpfer-2* and *proMpEF1:MpFER-Cit* #5 lines. See also Fig. S6.

pores (Fig. 7B), similar to what we observed when expressing the dominant-active *MpMRI^{R240C}* (Fig. S6A-C). This phenotype is reminiscent of the *quasimodo1* mutant in *A. thaliana*, in which cell walls have a reduced pectin content and cell adhesion is compromised (Bouton et al., 2002). Moreover, overexpression of *MpFER* affects the number of lobes in the antheridial receptacle, producing only four instead of eight lobes (Fig. S6H), supporting the importance of *MpFER* for sexual development. Considering the importance of *MpFER* for normal rhizoid formation, we also analyzed rhizoids in the *proMpEF1:MpFER-Cit* lines: although rhizoid morphology looked normal, a decrease in rhizoid number was observed (Fig. 7C,D). To analyze cell wall properties of *MpFER* overexpressor lines, chlorophyll efflux rates were measured as an indicator of epidermal permeability (Fig. 7E). Overexpression of *MpFER* clearly reduced the chlorophyll efflux compared with the wild type, whereas the opposite was observed in *Mpfer-2* mutants (Fig. 7E). Taken together, the results obtained by overexpressing *MpFER* support a role of *MpFER* in cell wall formation and the maintenance of tissue integrity during plant morphogenesis.

DISCUSSION

During land plant evolution, many developmental aspects have changed in order to adapt to new environments, producing the enormous diversity observed in the plant kingdom. However, the control and maintenance of CWI remained a key aspect for the biology of a plant cell. CWI sensing is not only important for vegetative growth by cell expansion, but it is also essential for sexual reproduction and defense responses.

The *CrRLK1L* family was first characterized for its importance during angiosperm fertilization, a process comprising aspects of polar cell elongation, CWI control, and cell-cell communication (Escobar-Restrepo et al., 2007; Huck et al., 2003; Rotman et al., 2003). Lately, different members of this family were found to carry

out diametrically opposite roles in diverse aspects of plant development, which has made it difficult to define the core or ancestral function of this gene family comprising 17-members in *A. thaliana* (Escobar-Restrepo et al., 2007; Hématy et al., 2007; Boisson-Dernier et al., 2009; Guo et al., 2009a,b; Kessler et al., 2010; Bai et al., 2014; Miyazaki et al., 2009; Keinath et al., 2010; Duan et al., 2010; Galindo-Trigo et al., 2020; Zhu et al., 2018; Li et al., 2015; Richter et al., 2017; Ge et al., 2017).

Here, we report the characterization of the single *CrRLK1L* gene encoded in the genome of *M. polymorpha*. Structurally, the *MpFER* ECD and kinase domain share similarities with previously characterized *CrRLK1L* members, including the malectin-like domain and conserved phosphorylation sites. Conservation of RALF and LRE members in *M. polymorpha* suggests that *MpFER* also forms a complex at the plasma membrane (Xiao et al., 2019). Although modeling predicted that the general structure of the complex was conserved, the interaction surfaces seem to have diverged and co-evolved independently in the respective lineages.

We observed a broad involvement of *MpFER* at both vegetative and reproductive stages of development. During vegetative growth of the gametophyte, *MpFER* is required for rhizoid formation and cell expansion, but it also plays a role in male gametogenesis and is expressed in female reproductive organs. These findings suggest that the *CrRLK1L*s have, also in ancestral land plants, held roles in various aspects of both vegetative and reproductive development. Thus, the role of *CrRLK1L*s in angiosperm reproduction does not represent a derived feature from a purely vegetative function in cell elongation in bryophytes but constitutes a conserved feature of this gene family.

Moreover, the almost ubiquitous expression of *MpFER* in *M. polymorpha* is consistent with the collective expression of different *CrRLK1L* members in essentially all tissues and organs of *A. thaliana* (Lindner et al., 2012). Thus, gene duplication allowed

the expansion of the *CrRLK1L* family in angiosperms, diversifying their expression patterns and functions but also leading to genetic redundancy (Boisson-Dernier et al., 2009; Galindo-Trigo et al., 2020; Ge et al., 2017; Lindner et al., 2012).

CrRLK1L members are important sensors of CWI during polarized growth, both in pollen tubes (Boisson-Dernier et al., 2009; Ge et al., 2017) and root hairs (Duan et al., 2010). In early divergent land plants, rhizoids are tip-growing cells with a function analogous to that of root hairs, important for taking up nutrients and water (Honkanen et al., 2016; Bowen, 1935). Based on the conservation of many genes controlling the development and growth of tip-growing cells forming rooting systems, it was suggested that these pathways were active in the earliest land plants that existed about 470 million years ago (Honkanen et al., 2016). That *MpFER* also controls rhizoid integrity points to the importance of the *CrRLK1L* pathway for polarized growth since the origin of land plants. Moreover, the fact that amorphic *Mpfer* mutants contain many dead cells demonstrates the importance of the *CrRLK1L* pathway for cellular integrity during vegetative growth. As the occurrence of dead cells was recently also reported in *Atfer-4* mutant seedlings (Malivert et al., 2021), the function of this pathway in maintaining cellular integrity may also be ancestral. Whether *MpFER* also plays a central role in plant innate immunity, as it does in angiosperms (Keinath et al., 2010; Stegmann et al., 2017), remains to be determined.

The signaling mechanisms downstream of *MpFER* in *M. polymorpha* development are still unclear. Mutations affecting *MpMRI*, the *M. polymorpha* ortholog of *AtMRI* that acts downstream of *AtFER* and *AtANX1/2* in *A. thaliana* during polarized growth (Boisson-Dernier et al., 2015), lead to a rhizoid phenotype similar to that of *Mpfer* (Honkanen et al., 2016; Westermann et al., 2019). The suppression of the rhizoid phenotype in *amiR-MpFER* transformants with the constitutively active form *MpMRI*^{R240C} corroborates a conserved *CrRLK1L* signaling cascade during polarized growth in *M. polymorpha*. However, whether this pathway also relies on Ca²⁺ and reactive oxygen species as second messengers, as it does in *A. thaliana*, remains to be determined.

In *A. thaliana*, loss-of-function mutations in the motor protein *AtKINESIN-13a*, a microtubule-based motor, cause cell elongation in petals, leaves and hypocotyls concomitant with changes in cell wall composition in leaves (Fujikura et al., 2014). This effect depends on functional *AtTHE1* and does not occur in *Atkinesin-13a Atthe1* double mutants. Interestingly, in this case, *AtTHE1* stimulates cell elongation in response to defects in cell wall deposition (Fujikura et al., 2014). Based on our results, we have no indication that *MpFER* acts as a CWI sensor and regulates growth similar to *AtTHE1* in response to cell wall disturbances. We have not observed a context in *M. polymorpha* development, in which *MpFER* inhibits cell expansion. Therefore, the ability to restrict growth in response to disturbances in CWI could represent an evolutionarily derived feature, as gene duplication allowed for the diversification and specialization of *CrRLK1Ls* to regulate cellular growth in a more complex and context-dependent way. The capacity to regulate growth flexibly appears to be fundamentally context dependent, as a similar discrepancy in promoting or inhibiting growth is also known for some well-studied growth-promoting agents, such as the phytohormones auxin and brassinosteroid, which can have growth-inhibitory effects dependent on tissue and concentration. The reverse was noted for the phytohormones ethylene and abscisic acid, which are usually considered growth inhibitors but can also promote growth, depending on the context (Pierik et al., 2006; Wolf and Höfte, 2014; Humplik et al., 2017).

Taken together, our results suggest an ancestral and conserved function of the *CrRLK1Ls* in polar cell growth and cell expansion, but also during sexual reproduction. In addition, we probed the relevance of *CrRLK1L* members for cell integrity and morphogenesis. In angiosperms, *CrRLK1Ls* occupy an important position at the interface of developmental and environmental inputs, which are integrated by a downstream signaling machinery that controls cell shape and polar growth to ensure normal development, e.g. by preventing cell rupture upon CWI defects. Whether the same downstream machinery is utilized in a similar fashion in *M. polymorpha* remains to be shown, even though the similarity in function points to a related mechanism. Even less is known about upstream aspects of *CrRLK1L* signaling. Future studies on the transcriptional regulation and the upstream components, such as the putative RALF ligand(s), in the highly simplified *M. polymorpha* system could provide fundamental insights into the molecular mechanism of the *CrRLK1L* pathway, which is so central to land plant physiology, growth and development.

MATERIALS AND METHODS

Experimental model

M. polymorpha subsp. *ruderalis* (Bischl. & Boissel.-Dub.) plants of the Tak-1 or Tak-2 accession were grown on sterile culture on half-strength Gamborg's B5 basal medium (PhytoTech Labs), supplemented with 1% phytoagar in Petri dishes sealed with air-permeable tape. The plants were kept under fluorescent light and long-day conditions (16 h light at 22°C, 8 h dark at 20°C) in Percival growth cabinets (models AR-41L3 and AR-41/L2). Alternatively, to induce sexual reproduction, plants were cultivated in Jiffy pots filled with a 1:1 mixture of soil ('Einheitserde D73+Bims', Universallerde) and sand or in culture boxes (Duchefa Eco2 Box, E1654) in sterile culture on half-strength Gamborg's B5 basal medium, under fluorescent light supplemented with far-red light (GreenPower LED module HF far-red, 929000464503 and 929000632103 Philips).

For *Arabidopsis thaliana* L. (Heyn), wild-type plants in all experiments were of the *Ler-0* accession. The *Atfer-2* mutant was obtained from the Signal Collection at the Salk Institute. Plants were grown in soil (ED73; Universallerde), covered with a thin quartz sand layer, under long photoperiods (16 h light/8 h dark) at 23°C and 60% relative humidity.

Phylogenetic analysis

Protein sequences were identified in plant genomes via BLASTp searches in <https://phytozome.jgi.doe.gov/pz/portal.html>. To elucidate the evolutionary relationship across land plant evolutionary history, we focused on *A. thaliana*, *Amborella trichopoda*, *Selaginella moellendorffii*, *Physcomitrium patens*, *Spagnum fallax*, *Ceratodon purpureus*, *Antoceros agrestis*, *A. punctatus* and *M. polymorpha* as representative species for angiosperms, lycophytes, mosses, hornworts and liverworts, respectively. Complete or partial coding protein sequences were aligned using ClustalW parameters and were conducted in MEGA7. Phylogenetic trees were constructed with the 'neighbor-joining' method, with a bootstrap test of 1000 replicates. The evolutionary distances were computed using the Poisson correction method.

Vector construction

Expression constructs

A BJ36 plasmid (Flores-Sandoval et al., 2015) containing a tripleVENUS-NLS (trpVNS) fragment was modified by adding a ligation-independent cloning (LiC) adapter site (De Rybel et al., 2011). A promoter fragment of *MpFER* of 3.2 kb was amplified by PCR using the primers listed in Table S2 and cloned into the BJ36 vector via LiC cloning. The *proMpFER* promoter fragment fused to trpVNS was then shuttled via *NotI* restriction sites into the HART01 (Flores-Sandoval et al., 2015) expression vector. The expression vector was also directly modified to contain the LiC sites, so promoter fragments could be directly cloned in front of trpVNS in the HART01 vector via LiC cloning. This vector was called VHL (trpVNS-containing HART01 vector with LiC sites).

amiRNA constructs

For functional analyses, three independent artificial microRNA (amiRNA) constructs were made (Fig. S2). The endogenous microRNA precursor *MpmiR160* was used as both backbone and template to design the constructs, which generated single species small RNA molecules of 21 nt length, complementary to the target gene transcript (Flores-Sandoval et al., 2016; Rövekamp et al., 2016). Three miR160 backbones containing independent amiR-MpFER/amiR-MpFER* duplexes were synthesized by GenScript and fused to the *pro*MpEF1 promoter in the BJ36 shuttle vector and shuttled to the HART01 expression vector as described previously (Rövekamp et al., 2016). The folding structure and design procedures have been explained in detail previously (Flores-Sandoval et al., 2016; Rövekamp et al., 2016). The sequences for the amiRNAs were designed to retain the exact physical properties of the endogenous *MpmiR160* template. The folding patterns were analyzed in Mfold software (Zuker, 2003) and the sequences synthesized (Fig. S2).

CRISPR/Cas gRNA

Selection of target sites was performed using CasFinder (Aach et al., 2014 preprint). Complementary oligos were designed and annealed for ligation into gRNA, in the pMpGE_En03 vector, previously digested with the BsaI restriction enzyme. Resulting gRNAs were incorporated into binary vector pMpGE011 through Gateway recombination.

Overexpression of MpFER and AtFER

The full-length MpFER sequence was amplified from genomic *M. polymorpha* DNA with attB sites and Gateway-cloned via pDONR207. For *A. thaliana* expression, MpFER was introduced into the expression vector pMDC201, which contains a *2X35S* promoter fragment and an in-frame C-terminal mGFP6 (Curtis and Grossniklaus, 2003). For *M. polymorpha* expression, MpFER was introduced into the binary vector pMpGWB308, which contains the *pro*MPEF1 promoter and an in-frame C-terminal Citrine (Ishizaki et al., 2015). Similarly, for expression of AtFER in *M. polymorpha*, the coding sequence of AtFER was introduced into the pMpGWB308 binary vector for the generation of the *pro*MpEF1:AtFER-Cit construct.

qRT-PCR and droplet digital PCR (ddPCR)

RNA extraction from *M. polymorpha*

RNA extraction from thallus tissue (~100 mg including apical notch) was carried out using the RNeasy Plant Mini Kit (74904, QIAGEN). To remove contaminating DNA, the TURBO DNA-free Kit (AM1907, Ambion) was used according to the manufacturer's recommendations. To extract RNA from the gametophores (two antheridiophores of >5 mm diameter were pooled, respectively, for each replicate), the Direct(-zol) RNA MiniPrep (R2050, ZymoResearch) was used with the TRIzol Reagent (15596026, Ambion) according to the manufacturer's protocol, including on-column DNase digestion and subsequent TURBO DNA-free Kit treatment. RNA samples were quantified using the Qubit RNA HS Assay Kit (Q32852, Life Technologies), a Nanodrop ND-1000 Spectrometer or an Agilent 2100 BioAnalyzer.

cDNA synthesis

cDNA was synthesized from 0.5 µg or 1.0 µg of total RNA. Reverse transcription was performed in 25 µl with 20 µg/ml Oligo(dT) 12-18 primers and 200 units of SuperScript II Reverse Transcriptase (18064-014, Invitrogen) according to the manufacturer's protocol. The resulting cDNA was diluted 1:9 by adding nuclease-free water. To control for genomic DNA contamination, control replicates of all samples were incubated without SuperScript II reverse transcriptase.

Primer tests and qRT-PCR

Primer efficiency and concentration tests were carried out for MpFER and suitable reference genes as described previously (Rövekamp et al., 2016; Althoff et al., 2014). Amplification experiments were carried out using a 7500 Applied Biosystem Fast Real-Time PCR System. Reactions were performed in 20 µl volumes containing 10 µl 2× SYBR Green Master Mix

(SsoAdvanced™ Universal SYBR Green Supermix), 200 nM (MpEF1 and MpFER) or 250 nM (MpACTIN) forward and reverse primers, and 1 µl diluted cDNA. Where possible, three technical and biological replicates were performed for each reaction. The primers used for qRT-PCR are summarized in Table S1.

ddPCR analysis

Individual PCR reactions were performed in a total volume of 25 µl, using 1× ddPCR EvaGreen Supermix, with droplets generated according to the manufacturer's recommendations. Reading of the PCR-amplified droplets was carried out using a QX200 Droplet Reader (Bio-Rad) and analyzed using QuantaSoft™ Software (v1.4, Bio-Rad). The counts from ddPCR were normalized through a log₂ transformation. Afterwards, relative expression was calculated against the geometric mean of the counts for all three reference genes (MpACT1, MpACT7 and MpAPT3) (Vandesompele et al., 2002): [log₂(gene tested+1)–log₂(geom. mean of all references+1)]. The primers used for the ddPCR are summarized in Table S1.

3' RACE-PCR

RNA from wild-type and *Mpfer-1* mutant plants were extracted as previously described. A poly(G)-tail was added at the 3' end of the RNA according to a Poly(A) Polymerase protocol (Thermo Scientific), using GTP instead of ATP. Reverse transcription was performed using anchored Oligo(dC) instead of Oligo(dT). Nested PCR on the cDNA was performed using two forward primers that matched the 3' UTR sequence of MpFER (3' RACE-Fwd1 and 3' RACE-Fwd2) and Oligo(dC) that are listed in Table S1. PCR fragments were purified and sequenced.

Transformation of *M. polymorpha* and *A. thaliana*

Agrobacterium-mediated transformation using regenerating thalli of *M. polymorpha* was performed by co-cultivation of 15-day-old plant fragments with transformed *Agrobacterium tumefaciens* (GV3101) cells (Kubota et al., 2013; Ishizaki et al., 2008). After 3 days of incubation, positive transformants were selected on Gomborg's B5 plates supplemented with 10 µg/ml hygromycin B (Invitrogen), 0.5 µM chlorosulfuron or kanamycin, and 100 µg/ml of cefotaxime sodium. Isogenic lines were obtained using plants derived from gemmae of the T1 generation (G1 generation). G1 or subsequent gemmae generations were used for all experiments, as they are derived from single cells (Barnes and Land, 1907; Hughes, 1971). Transformation of *A. thaliana* via *A. tumefaciens* (GV3101) was performed by floral dipping according to the method of Bent (2006). Primers used for amplification of promoter fragments of MpFER are listed in Table S2.

Microscopy

Plants were observed in a Lumar.V12 (ZEISS) or a Leica MZFLIII dissection microscope and imaged with an Axiocam HRc (ZEISS) or Leica DFC 420C camera. Clearings were observed using a Leica DMR microscope and photographed with an Axiocam 105 color camera. Fluorescence reporter expression was analyzed using a Leica SP5 confocal microscope. Fiji (Schindelin et al., 2012) and GIMP (version 2.8.10) software were used for adjustments of brightness, contrast, channel selection and image size.

Tissue clearing for brightfield microscopy

M. polymorpha tissues were fixed in Carnoy's solution and incubated at 4°C overnight, followed by rehydration in an ethanol (EtOH) series of 85%, 70%, 50% and 30%. Samples were incubated for 1 h at 4°C for each step and then incubated in chloral hydrate solution at 4°C overnight. Samples were mounted in chloral hydrate.

Calcofluor White staining for cell size measurements

Pieces of fresh thallus tissue located in fully differentiated zones (Solly et al., 2017) of plants grown on plates were dissected out and put into water. The pieces were transferred to PBS pH 6.1 containing 100 µg/ml Calcofluor White and vacuum-infiltrated for 1 h before being mounted on slides. The area of the epidermal cells was measured using Imaris 8.3.1. software (Bitplane AG). Cells of air pores and the two adjacent cell layers were excluded from the analysis, as well as the spiraling cells surrounding newly developing air pores.

Cell death staining

Seven-day-old gemmalings were stained with lactophenol-Trypan Blue (10 ml of lactic acid, 10 ml of glycerol, 10 g of phenol, 10 mg of Trypan Blue, dissolved in 10 ml of distilled water) by boiling them for approximately 1 min in the stain solution and then decolorized in chloral hydrate (2.5 g of chloral hydrate dissolved in 1 ml of distilled water) for at least 30 min. They were mounted in chloral hydrate and imaged using a dissection microscope.

Scanning electron microscopy

Twenty-day-old plants of wild type and *proMpEF1:MpFER-Cit* lines #5 and #9 were harvested and fixed in glutaraldehyde (0.25% in 20 mM HEPES) overnight at 4°C. After fixation, dehydration with an acetone series (from 50% to 100% acetone ‘ultradry’) was carried out. The samples were then critical-point dried, without the following sputter-coating step. Microscopic imaging was performed on a JSM-6010 scanning electron microscope (JEOL) at the Center for Microscopy and Image Analysis at the University of Zurich.

Cellular force microscopy

To evaluate the stiffness of the gemmaling tissue, we used cellular force microscopy (Felekis et al., 2011; Vogler et al., 2013). A microelectromechanical systems (MEMS)-based FT-S100 force sensor (FemtoTools AG) with a glued-on tungsten probe (T-4-22; Picoprobe by GGB Industries) was used to indent the gemmaling tissue. The sensor has a force range of ± 100 μ N and a resolution of 15 nN measured at 500 Hz. The sensor was attached with a custom-made acrylic arm to an *xyz* positioner (SLC-2460-M, SmarAct), which was fixed on an *xyz* piezo stage (P-563.3CD PIMars; Physik Instrumente). The *xyz* positioner was used for the rough positioning of the sensor on a part of a gemma that was as much as possible in contact with the supporting glass slide and away from the meristematic zones. Nine evenly spaced measurements were then taken in a 3×3 grid, again using the *xyz* positioner to place the sensor, while the indentation at each position was driven by the piezo stage. This procedure was repeated a second time on each gemmaling, whenever possible on the opposite lobe.

The stiffness analysis was achieved with MATLAB (MathWorks) based on the slope fitted to the force-displacement curves, which were acquired by cellular force microscopy. In a first round of data curation, each force-indentation curve was visually inspected, and curves that did not have a clear contact point or showed a clear displacement of the gemmaling, indicated by an irregular slope, were discarded. The remaining data exhibited a bimodal distribution with a high density at very soft values around 1 μ N, indicating the presence of an artifact due to gemmalings that were not in contact with the slide and, therefore, were displaced rather than indented. To identify such failed measurements, we pooled all data and fitted a Gaussian mixture model with two components. We then removed all measurements that were closer than three standard deviations to the mean of the distribution with the smallest mean (mean=1.16 μ N and s.d.=0.56 μ N). Hence, all measurements with a value below 2.9 μ N were removed.

Boxplots and statistical analysis were performed in MATLAB. The statistical tests used to assess the significance of differences between groups are indicated in the figure legends.

Western blot analysis

M. polymorpha explants were ground in liquid nitrogen and resuspended in 300 μ l of Laemmli buffer (Laemmli, 1970). After centrifugation at 6000 rpm (3800 g) for 5 min at 4°C, the supernatant was recovered. Protein accumulation was confirmed by western blotting using an anti-GFP antibody (1:3000; TP401, Torrey Pines Biolabs). As secondary antibody, a goat anti-rabbit antibody (1:20,000; S09602, Agrisera) was used followed by ECL detection using the FUSION FX - Western Blot & Chemi Imaging system (Vilber Lourmat).

Growth rate experiments

Gemmae of wild-type, *Mpfer-1* and independent transformation lines of *amiR-MpFER* lines were grown on plates and the thallus area was measured

over time. Ten or 30 gemmae of four independent transformation lines were grown on half-strength Gamborg’s B5 and scanned on an Epson 2450 Photo scanner at 600 dpi. Plant area was measured using color threshold settings and particle analysis in Fiji software (Schindelin et al., 2012).

Expression map

Gene expression of *CrRLK1L* signaling pathway components was calculated from publicly available RNA-seq data of 39 samples of *M. polymorpha* Tak-1 and Tak-2. Samples were grouped by tissue and analyzed under the same pipeline: Nextera paired-end adapters were trimmed from sequencing reads using the bbdut tool embedded in the BBDMap software package (Bushnell, 2014). Read ends with quality below 20 were also trimmed and the minimum read length was set to 25. The rest of parameters of bbdut were set at default values. Reads were mapped to *M. polymorpha* reference genome (v3.1) (Bowman et al., 2017) using the TopHat software (v2.1.1) (Trapnell et al., 2009), designed for RNA-sequencing read mapping. TopHat contains Bowtie (v2.3.2.0) (Langdon, 2015) as the aligner software. All parameters were set to default values except for the RAM memory and number of used Cores. Mapped reads were sorted using samtools (v1.3.1) (Li et al., 2009) and counted with the software HTSeq-count (v0.9.1) (Anders et al., 2015). Gene expression values were calculated using the package DESeq2 (Release 3.6) (Love et al., 2014) for R software (v3.4.4) (<https://www.R-project.org/>). Another R package, ggplot2 (release 2.2.1) (Wickham, 2016), was used for producing the figures. A summary of the samples that were used in this study is provided in Table S3.

Chlorophyll efflux rate

To measure the chlorophyll efflux rate (Lolle et al., 1997), 10-day-old gemmalings were used. Sixteen replicates of *MpFER*-overexpressor, *Mpfer-2* mutant, and wild-type lines were immersed in an 80% EtOH solution in 5-ml tubes. The tubes were agitated gently on a shaker platform. Aliquots of 2 μ l were removed every minute, during the first 10 min. The amount of chlorophyll extracted by the EtOH solution was quantified with a spectrophotometer (NanoDrop 8000, Thermo Fisher Scientific) and calculated from UV light absorption at 647 and 664 nm. The micromolar concentration of total chlorophyll per gram of fresh weight of tissue per ml of EtOH was calculated using the following equation: total micromoles chlorophyll=7.93(A_{664})+19.53(A_{647}).

3D protein structure modeling

Comparative modeling of protein 3D structures was performed using the SWISS-MODEL online tool (Schwede et al., 2003). The software was fed with the three protein sequences of *MpFER*, *MpRALF1* and *MpLRE1* as input to model. The templates chosen for modeling the three sequences were selected from the best homology result provided by SWISS-MODEL (Table S4). Quality control of the model was assessed using the same tool and the results are summarized in Table S4. Spatial comparisons of the *M. polymorpha* predicted structures with the crystal structures of *A. thaliana* were performed in PyMOL (DeLano, 2002).

Quantification and statistical analysis

Analyses were performed in InfoStat (<http://www.infostat.com.ar>), the R base package and MATLAB. Statistical tests are indicated in the corresponding figure legend.

Acknowledgements

We thank Liam Dolan for kindly providing the *Mpfer-1/Mpthe* mutant, Valeria Gagliardini for help with qRT-PCR and ddPCR, Anja Grossniklaus for help in measuring epidermal cell area, Célia Baroux and Ethel Mendocillo-Sato for instructions on confocal microscopy and the use of the Imaris software, Tiago Meier for helping with sample preparation for scanning electron microscopy, Isabel Monte and Cyril Zipfel for comments on the manuscript, and Christof Eichenberger, Frédérique Pasquer, Arturo Bolaños, Daniela Guthörl, Daniel Prata, and Peter Kopf for general lab support.

Competing interests

The authors declare no competing or financial interests.

Author contributions

Conceptualization: M.A.M., M.R., U.G.; Methodology: M.A.M., M.R.; Software: A.G.-F.; Validation: M.A.M., M.R., A.G.-F., D.M., P.G., H.V., D.L., J.L.B., U.G.; Formal analysis: M.A.M., M.R., A.G.-F., D.M., P.G., H.V., U.G.; Investigation: M.A.M., M.R., D.M., P.G., H.V., D.L.; Resources: J.L.B., U.G.; Data curation: A.G.-F.; Writing - original draft: M.A.M., M.R., A.G.-F., U.G.; Writing - review & editing: M.A.M., M.R., A.G.-F., D.M., P.G., H.V., J.L.B., U.G.; Visualization: M.A.M., M.R., A.G.-F.; Supervision: J.L.B., U.G.; Project administration: U.G.; Funding acquisition: M.R., J.L.B., U.G.

Funding

This work was supported by the Universität Zürich and Monash University, and by grants from the Forschungskredit of the University of Zurich (FK-16-090 to M.R.), the Australian Research Council (DP130100177 to J.L.B.) and the Schweizerischer Nationalfonds zur Förderung der Wissenschaftlichen Forschung (310030B 160336 and 31003A_179553 to U.G.).

Peer review history

The peer review history is available online at <https://journals.biologists.com/dev/lookup/doi/10.1242/dev.200580.reviewer-comments.pdf>.

References

- Aach, J., Mali, P. and Church, G. M. (2014). CasFinder: flexible algorithm for identifying specific Cas9 targets in genomes. *bioRxiv* doi:10.1101/005074
- Althoff, F., Kopischke, S., Zobell, O., Ide, K., Ishizaki, K., Kohchi, T. and Zachgo, S. (2014). Comparison of the *MpEF1α* and *CaMV35* promoters for application in *Marchantia polymorpha* overexpression studies. *Transgenic Res.* **23**, 235-244. doi:10.1007/s11248-013-9746-z
- Anders, S., Pyl, P. T. and Huber, W. (2015). HTSeq – a Python framework to work with high-throughput sequencing data. *Bioinformatics* **31**, 166-169. doi:10.1093/bioinformatics/btu638
- Bai, L., Ma, X., Zhang, G., Song, S., Zhou, Y., Gao, L., Miao, Y. and Song, C.-P. (2014). A receptor-like kinase mediates ammonium homeostasis and is important for the polar growth of root hairs in *Arabidopsis*. *Plant Cell* **26**, 1497-1511. doi:10.1105/tpc.114.124586
- Barnes, C. R. and Land, W. J. G. (1907). Bryological papers. I. The origin of air chambers. *Bot Gaz* **44**, 197-213. doi:10.1086/329317
- Baumberger, N., Ringli, C. and Keller, B. (2001). The chimeric leucine-rich repeat/ extensin cell wall protein LRX1 is required for root hair morphogenesis in *Arabidopsis thaliana*. *Genes Dev.* **15**, 1128-1139. doi:10.1101/gad.200201
- Bent, A. (2006). *Agrobacterium Protocols*. Vol. 1, 2nd edn. Totowa, NJ: Humana Press.
- Boisson-Dernier, A., Roy, S., Kritsas, K., Grobei, M. A., Jaciubek, M., Schroeder, J. I. and Grossniklaus, U. (2009). Disruption of the pollen-expressed *FERONIA* homologs *ANXUR1* and *ANXUR2* triggers pollen tube discharge. *Development* **136**, 3279-3288. doi:10.1242/dev.040071
- Boisson-Dernier, A., Kessler, S. A. and Grossniklaus, U. (2011). The walls have ears: the role of plant CrRLK1Ls in sensing and transducing extracellular signals. *J. Exp. Bot.* **62**, 1581-1591. doi:10.1093/jxb/erq445
- Boisson-Dernier, A., Franck, C. M., Lituiev, D. S. and Grossniklaus, U. (2015). Receptor-like cytoplasmic kinase MARIS functions downstream of CrRLK1L-dependent signaling during tip growth. *Proc. Natl. Acad. Sci. USA* **112**, 12211-12216. doi:10.1073/pnas.1512375112
- Bouton, S., Leboeuf, E., Mouille, G., Leydecker, M.-T., Talbot, J., Granier, F., Lahaye, M., Höfte, H. and Truong, H.-N. (2002). *QUASIMODO1* encodes a putative membrane-bound glycosyltransferase required for normal pectin synthesis and cell adhesion in *Arabidopsis*. *Plant Cell* **14**, 2577-2590. doi:10.1105/tpc.004259
- Bowen, E. J. (1935). A note on the conduction of water in *Fimbraria bleumeana*. *Ann. Bot.* **49**, 844-848. doi:10.1093/oxfordjournals.aob.a090540
- Bowman, J. L., Floyd, S. K. and Sakakibara, K. (2007). Green genes-comparative genomics of the green branch of life. *Cell* **129**, 229-234. doi:10.1016/j.cell.2007.04.004
- Bowman, J. L., Araki, T., Arteaga-Vazquez, M. A., Berger, F., Dolan, L., Haseloff, J., Ishizaki, K., Kyoizaki, J., Lin, S.-S., Nagasaka, H., et al. (2016). The naming of names: guidelines for gene nomenclature in *Marchantia*. *Plant Cell Physiol.* **57**, 257-261. doi:10.1093/pcp/pcv193
- Bowman, J. L., Kohchi, T., Yamato, K. T., Jenkins, J., Shu, S., Ishizaki, K., Yamaoka, S., Nishihama, R., Nakamura, Y., Berger, F. et al. (2017). Insights into land plant evolution garnered from the *Marchantia polymorpha* genome. *Cell* **171**, 287-304.e15. doi:10.1016/j.cell.2017.09.030
- Bushnell, B. (2014). *BBMap: a fast, accurate, splice-aware aligner* (No. LBNL-7065E). Berkeley, CA, US: Lawrence Berkeley Natl. Lab/LBNL.
- Capron, A., Gourgues, M., Neiva, L. S., Faure, J.-E., Berger, F., Pagnussat, G., Krishnan, A., Alvarez-Mejia, C., Vielle-Calzada, J.-P., Lee, Y.-R., et al. (2008). Maternal control of male-gamete delivery in *Arabidopsis* involves a putative GPI-anchored protein encoded by the *LORELEI* gene. *Plant Cell* **20**, 3038-3049. doi:10.1105/tpc.108.061713
- Cheung, A. Y. and Wu, H.-M. (2011). THESEUS 1, FERONIA and relatives: a family of cell wall-sensing receptor kinases? *Curr. Opin. Plant Biol.* **14**, 632-641. doi:10.1016/j.pbi.2011.09.001
- Chiyoda, S., Ishizaki, K., Kataoka, H., Yamato, K. T. and Kohchi, T. (2008). Direct transformation of the liverwort *Marchantia polymorpha* L. by particle bombardment using immature thalli developing from spores. *Plant Cell Rep.* **27**, 1467-1473. doi:10.1007/s00299-008-0570-5
- Curtis, M. D. and Grossniklaus, U. (2003). A Gateway cloning vector set for high-throughput functional analysis of genes in *planta*. *Plant Physiol.* **133**, 462-469. doi:10.1104/pp.103.027979
- De Rybel, B., van den Berg, W., Lokere, A. S., Liao, C.-Y., van Mourik, H., Möller, B., Llavata-Peris, C. I. and Weijers, D. (2011). A versatile set of ligation-independent cloning vectors for functional studies in plants. *Plant Physiol.* **156**, 1292-1299. doi:10.1104/pp.111.177337
- DeLano, W. L. (2002). Pymol: an open-source molecular graphics tool. *CCP4 Newsl. Protein Crystallogr.* **40**, 82-92.
- Denness, L., McKenna, J. F., Segonzac, C., Wormit, A., Madhou, P., Bennett, M., Mansfield, J., Zipfel, C. and Hamann, T. (2011). Cell wall damage-induced lignin biosynthesis is regulated by a reactive oxygen species- and jasmonic acid-dependent process in *Arabidopsis*. *Plant Physiol.* **156**, 1367-1374. doi:10.1104/pp.111.175737
- Deslauriers, S. D. and Larsen, P. B. (2010). FERONIA is a key modulator of brassinosteroid and ethylene responsiveness in *Arabidopsis* hypocotyls. *Mol. Plant* **3**, 626-640. doi:10.1093/mp/ssp015
- Duan, Q., Kita, D., Li, C., Cheung, A. Y. and Wu, H.-M. (2010). FERONIA receptor-like kinase regulates RHO GTPase signaling of root hair development. *Proc. Natl. Acad. Sci. USA* **107**, 17821-17826. doi:10.1073/pnas.1005366107
- Dünser, K., Gupta, S., Herger, A., Feraru, M. I., Ringli, C. and Kleine-Vehn, J. (2019). Extracellular matrix sensing by FERONIA and Leucine-Rich Repeat Extensins controls vacuolar expansion during cellular elongation in *Arabidopsis thaliana*. *EMBO J.* **38**, e100353. doi:10.15252/embj.2018100353
- Escobar-Restrepo, J.-M., Huck, N., Kessler, S., Gagliardini, V., Gheyselinck, J., Yang, W.-C. and Grossniklaus, U. (2007). The FERONIA receptor-like kinase mediates male-female interactions during pollen tube reception. *Science* **317**, 656-660. doi:10.1126/science.1143562
- Felekis, D., Muntwyler, S., Vogler, H., Beyeler, F., Grossniklaus, U. and Nelson, B. J. (2011). Quantifying growth mechanics of living, growing plant cells *in situ* using microrobotics. *Micro Nano Lett.* **6**, 311-316. doi:10.1049/mnl.2011.0024
- Feng, W., Kita, D., Peaucelle, A., Cartwright, H. N., Doan, V., Duan, Q., Liu, M.-C., Maman, J., Steinhilber, L., Schmitz-Thom, I., et al. (2018). The FERONIA receptor kinase maintains cell-wall integrity during salt stress through Ca²⁺ signaling. *Curr. Biol.* **28**, 666-675.e5. doi:10.1016/j.cub.2018.01.023
- Flores-Sandoval, E., Eklund, D. M. and Bowman, J. L. (2015). A simple auxin transcriptional response system regulates multiple morphogenetic processes in the liverwort *Marchantia polymorpha*. *PLoS Genet.* **11**, e1005207. doi:10.1371/journal.pgen.1005207
- Flores-Sandoval, E., Dierschke, T., Fisher, T. J. and Bowman, J. L. (2016). Efficient and inducible use of artificial microRNAs in *Marchantia polymorpha*. *Plant Cell Physiol.* **57**, 281-290. doi:10.1093/pcp/pcv068
- Floyd, S. K. and Bowman, J. L. (2007). The ancestral developmental tool kit of land plants. *Int. J. Plant Sci.* **168**, 1-35. doi:10.1086/509079
- Franck, C. M., Westermann, J. and Boisson-Dernier, A. (2018). Plant malectin-like receptor kinases: from cell wall integrity to immunity and beyond. *Annu. Rev. Plant Biol.* **69**, 301-328. doi:10.1146/annurev-arplant-042817-040557
- Fujikura, U., Einsaesser, L., Breuninger, H., Sánchez-Rodríguez, C., Ivakov, A., Laux, T., Findlay, K., Persson, S. and Lenhard, M. (2014). Atkinesin-13A modulates cell-wall synthesis and cell expansion in *Arabidopsis thaliana* via the *THESEUS1* pathway. *PLoS Genet.* **10**, e1004627. doi:10.1371/journal.pgen.1004627
- Gachomo, E. W., Jno Baptiste, L., Kefela, T., Saidel, W. M. and Kotchoni, S. O. (2014). The *Arabidopsis* *CURVY1* (*CVY1*) gene encoding a novel receptor-like protein kinase regulates cell morphogenesis, flowering time and seed production. *BMC Plant Biol.* **14**, 221. doi:10.1186/s12870-014-0221-7
- Galindo-Trigo, S., Gray, J. E. and Smith, L. M. (2016). Conserved roles of CrRLK1L receptor-like kinases in cell expansion and reproduction from Algae to Angiosperms. *Front. Plant Sci.* **7**, 1269. doi:10.3389/fpls.2016.01269
- Galindo-Trigo, S., Blanco-Touriñán, N., DeFalco, T. A., Wells, E. S., Gray, J. E., Zipfel, C. and Smith, L. M. (2020). CrRLK1L receptor-like kinases HERK1 and ANJEA are female determinants of pollen tube reception. *EMBO Rep.* **21**, e48466. doi:10.15252/embr.201948466
- Ge, Z., Bergonci, T., Zhao, Y., Zou, Y., Du, S., Liu, M.-C., Luo, X., Ruan, H., García-Valencia, L. E., Zhong, S. et al. (2017). *Arabidopsis* pollen tube integrity and sperm release are regulated by RALF-mediated signaling. *Science* **358**, 1596-1600. doi:10.1126/science.aao3642
- Ginanjar, E. F., Teh, O.-K. and Fujita, T. (2021). Characterisation of rapid alkalisation factors in *Physcomitrium patens* reveals functional conservation in tip growth. *New Phytol.* **233**, 2442-2457. doi:10.1111/nph.17942
- Gonneau, M., Desprez, T., Martin, M., Doblaz, V. G., Bacete, L., Miart, F., Sormani, R., Hématy, K., Renou, J., Landrein, B. et al. (2018). Receptor kinase

- THESEUS1 is a RAPID ALKALINIZATION FACTOR34 receptor in *Arabidopsis*. *Curr. Biol.* **28**, 2452-2458.e4. doi:10.1016/j.cub.2018.05.075
- Guo, H., Li, L., Ye, H., Yu, X., Algreen, A. and Yin, Y. (2009a). Three related receptor-like kinases are required for optimal cell elongation in *Arabidopsis thaliana*. *Proc. Natl. Acad. Sci. USA* **106**, 7648-7653. doi:10.1073/pnas.0812346106
- Guo, H., Ye, H., Li, L. and Yin, Y. (2009b). A family of receptor-like kinases are regulated by BES1 and involved in plant growth in *Arabidopsis thaliana*. *Plant Signal. Behav.* **4**, 784-786. doi:10.4161/psb.4.8.9231
- Haruta, M., Sabat, G., Stecker, K., Minkoff, B. B. and Sussman, M. R. (2014). A peptide hormone and its receptor protein kinase regulate plant cell expansion. *Science* **343**, 408-411. doi:10.1126/science.1244454
- Hématy, K. and Höfte, H. (2008). Novel receptor kinases involved in growth regulation. *Curr. Opin. Plant Biol.* **11**, 321-328. doi:10.1016/j.pbi.2008.02.008
- Hématy, K., Sado, P.-E., Van Tuinen, A., Rochange, S., Desnos, T., Balzergue, S., Pelletier, S., Renou, J.-P. and Höfte, H. (2007). A receptor-like kinase mediates the response of *Arabidopsis* cells to the inhibition of cellulose synthesis. *Curr. Biol.* **17**, 922-931. doi:10.1016/j.cub.2007.05.018
- Hirano, N., Marukawa, Y., Abe, J., Hashiba, S., Ichikawa, M., Tanabe, Y., Ito, M., Nishii, I., Tsuchikane, Y. and Sekimoto, H. (2015). A Receptor-like kinase, related to cell wall sensor of higher plants, is required for sexual reproduction in the unicellular Charophycean alga, *Closterium peracerosum-strigosum-littorale* complex. *Plant Cell Physiol.* **56**, 1456-1462. doi:10.1093/pcp/pcv065
- Honkanen, S., Jones, V. A. S., Morieri, G., Champion, C., Hetherington, A. J., Kelly, S., Proust, H., Saint-Marcoux, D., Prescott, H. and Dolan, L. (2016). The mechanism forming the cell surface of tip-growing rooting cells is conserved among land plants. *Curr. Biol.* **26**, 3238-3244. doi:10.1016/j.cub.2016.09.062
- Huck, N., Moore, J. M., Federer, M. and Grossniklaus, U. (2003). The *Arabidopsis* mutant *feronia* disrupts the female gametophytic control of pollen tube reception. *Development* **130**, 2149-2159. doi:10.1242/dev.00458
- Hughes, S. J. (1971). On conidia of fungi, and gemmae of algae, bryophytes, and pteridophytes. *Can. J. Bot.* **49**, 1319-1339. doi:10.1139/b71-187
- Humplik, J. F., Bergougnoux, V. and Van Volkenburgh, E. (2017). To stimulate or inhibit? That is the question for the function of abscisic acid. *Trends Plant Sci.* **22**, 830-841. doi:10.1016/j.tplants.2017.07.009
- Ishizaki, K. (2017). Evolution of land plants: insights from molecular studies on basal lineages. *Biosci. Biotechnol. Biochem.* **81**, 73-80. doi:10.1080/09168451.2016.1224641
- Ishizaki, K., Chiyoda, S., Yamato, K. T. and Kohchi, T. (2008). *Agrobacterium*-mediated transformation of the haploid liverwort *Marchantia polymorpha* L., an emerging model for plant biology. *Plant Cell Physiol.* **49**, 1084-1091. doi:10.1093/pcp/pcn085
- Ishizaki, K., Nishihama, R., Ueda, M., Inoue, K., Ishida, S., Nishimura, Y., Shikanai, T. and Kohchi, T. (2015). Development of gateway binary vector series with four different selection markers for the liverwort *Marchantia polymorpha*. *PLoS ONE* **10**, e0138876. doi:10.1371/journal.pone.0138876
- Keinath, N. F., Kierszniowska, S., Lorek, J., Bourdais, G., Kessler, S. A., Shimosato-Asano, H., Grossniklaus, U., Schulze, W. X., Robatzek, S. and Panstruga, R. J. (2010). PAMP (pathogen-associated molecular pattern)-induced changes in plasma membrane compartmentalization reveal novel components of plant immunity. *J. Biol. Chem.* **285**, 39140-39149. doi:10.1074/jbc.M110.160531
- Kenrick, P. and Crane, P. R. (1997). The origin and early evolution of plants on land. *Nature* **389**, 33-39. doi:10.1038/37918
- Kessler, S. A., Shimosato-Asano, H., Keinath, N. F., Wuest, S. E., Ingram, G., Panstruga, R. and Grossniklaus, U. (2010). Conserved molecular components for pollen tube reception and fungal invasion. *Science* **330**, 968-971. doi:10.1126/science.1195211
- Kessler, S. A., Lindner, H., Jones, D. S. and Grossniklaus, U. (2014). Functional analysis of related CrRLK1L receptor-like kinases in pollen tube reception. *EMBO Rep.* **16**, 107-115. doi:10.15252/embr.201438801
- Kim, C. M. and Dolan, L. (2016). ROOT HAIR DEFECTIVE SIX-LIKE class I genes promote root hair development in the grass *Brachypodium distachyon*. *PLoS Genet.* **12**, e1006211. doi:10.1371/journal.pgen.1006211
- Kubota, A., Ishizaki, K., Hosaka, M. and Kohchi, T. (2013). Efficient *Agrobacterium*-mediated transformation of the liverwort *Marchantia polymorpha* using regenerating thalli. *Biosci. Biotechnol. Biochem.* **77**, 167-172. doi:10.1271/bbb.120700
- Laemmli, U. K. (1970). Cleavage of structural proteins during the assembly of the head of bacteriophage T4. *Nature* **227**, 680-685. doi:10.1038/227680a0
- Langdon, W. B. (2015). Performance of genetic programming optimised Bowtie2 on genome comparison and analytic testing (GCAT) benchmarks. *BioData Min.* **8**, 1. doi:10.1186/s13040-014-0034-0
- Li, H., Handsaker, B., Wysoker, A., Fennell, T., Ruan, J., Homer, N., Marth, G., Abecasis, G. and Durbin, R. (2009). The sequence alignment/map format and SAMtools. *Bioinformatics* **25**, 2078-2079. doi:10.1093/bioinformatics/btp352
- Li, C., Yeh, F.-L., Cheung, A. Y., Duan, Q., Kita, D., Liu, M.-C., Maman, J., Luu, E. J., Wu, B. W., Gates, L. et al. (2015). Glycosylphosphatidylinositol-anchored proteins as chaperones and co-receptors for FERONIA receptor kinase signaling in *Arabidopsis*. *eLife* **4**, e06587. doi:10.7554/eLife.06587.031
- Liao, H.-Z., Zhu, M.-M., Cui, H.-H., Du, X.-Y., Tang, Y., Chen, L.-Q., Ye, D. and Zhang, X.-Q. (2016). MARI5 plays important roles in *Arabidopsis* pollen tube and root hair growth. *J. Integr. Plant Biol.* **58**, 927-940. doi:10.1111/jipb.12484
- Lin, W., Tang, W., Pan, X., Huang, A., Gao, X., Anderson, C. T. and Yang, Z. (2021). *Arabidopsis* pavement cell morphogenesis requires FERONIA binding to pectin for activation of ROP GTPase signaling. *Curr. Biol.* **32**, 497-507.e4. doi:10.1016/j.cub.2021.11.030
- Lindner, H., Müller, L. M., Boisson-Dernier, A. and Grossniklaus, U. (2012). CrRLK1L receptor-like kinases: not just another brick in the wall. *Curr. Opin. Plant Biol.* **15**, 659-669. doi:10.1016/j.pbi.2012.07.003
- Liu, L., Zheng, C., Kuang, B., Wei, L., Yan, L. and Wang, T. (2016). Receptor-like kinase RUP0 interacts with potassium transporters to regulate pollen tube growth and integrity in rice. *PLoS Genet.* **12**, e1006085. doi:10.1371/journal.pgen.1006085
- Lolle, S. J., Berlyn, G. P., Engstrom, E. M., Krolikowski, K. A., Reiter, W.-D. and Pruitt, R. E. (1997). Developmental regulation of cell interactions in the *Arabidopsis fiddlehead-1* mutant: a role for the epidermal cell wall and cuticle. *Dev. Biol.* **189**, 311-321. doi:10.1006/dbio.1997.8671
- Love, M. I., Huber, W. and Anders, S. (2014). Moderated estimation of fold change and dispersion for RNA-seq data with DESeq2. *Genome Biol.* **15**, 550. doi:10.1186/s13059-014-0550-8
- Malivert, A., Erguvan, Ö., Chevallier, A., Dehem, A., Friaud, R., Liu, M., Martin, M., Peyraud, T., Hamant, O. and Verger, S. (2021). FERONIA and microtubules independently contribute to mechanical integrity in the *Arabidopsis* shoot. *PLoS Biol.* **19**, e3001454. doi:10.1371/journal.pbio.3001454
- Mao, D., Yu, F., Li, J., Van de Poel, B., Tan, D., Li, J., Liu, Y., Li, X., Dong, M., Chen, L. et al. (2015). FERONIA receptor kinase interacts with S-adenosylmethionine synthetase and suppresses S-adenosylmethionine production and ethylene biosynthesis in *Arabidopsis*. *Plant Cell Env.* **38**, 2566-2574. doi:10.1111/pce.12570
- Mecchia, M. A., Santos-Fernandez, G., Duss, N. N., Somoza, S. C., Boisson-Dernier, A., Gagliardini, V., Martínez-Bernardini, A., Fabrice, T. N., Ringli, C., Muschietti, J. P. et al. (2017). RALF4/19 peptides interact with LRX proteins to control pollen tube growth in *Arabidopsis*. *Science* **358**, 1600-1603. doi:10.1126/science.aao5467
- Merz, D., Richter, J., Gonneau, M., Sanchez-Rodriguez, C., Eder, T., Sormani, R., Martin, M., Hématy, K., Höfte, H. and Hauser, M.-T. (2017). T-DNA alleles of the receptor kinase THESEUS1 with opposing effects on cell wall integrity signaling. *J. Exp. Bot.* **68**, 4583-4593. doi:10.1093/jxb/erx263
- Mishler, B. D. and Churchill, S. P. (1984). A cladistic approach to the phylogeny of the 'bryophytes'. *Brittonia* **36**, 406-424. doi:10.2307/2806602
- Miyazaki, S., Murata, T., Sakurai-Ozato, N., Kubo, M., Demura, T., Fukuda, H. and Hasebe, M. (2009). ANXUR1 and 2, sister genes to FERONIA/SIKRENE, are male factors for coordinated fertilization. *Curr. Biol.* **19**, 1327-1331. doi:10.1016/j.cub.2009.06.064
- Ngo, Q. A., Vogler, H., Lituiev, D. S., Nestorova, A. and Grossniklaus, U. (2014). A calcium dialog mediated by the FERONIA signal transduction pathway controls plant sperm delivery. *Dev. Cell* **29**, 491-500. doi:10.1016/j.devcel.2014.04.008
- Nishiyama, T., Fujita, T., Shin-I, T., Seki, M., Nishide, H., Uchiyama, I., Kamiya, A., Carninci, P., Hayashizaki, Y., Shinozaki, K. et al. (2003). Comparative genomics of *Physcomitrella patens* gametophytic transcriptome and *Arabidopsis thaliana*: implication for land plant evolution. *Proc. Natl. Acad. Sci. USA* **100**, 8007-8012. doi:10.1073/pnas.0932694100
- Nissen, K. S., Willats, W. G. T. and Malinovsky, F. G. (2016). Understanding CrRLK1L function: cell walls and growth control. *Trends Plant Sci.* **21**, 516-527. doi:10.1016/j.tplants.2015.12.004
- Okuda, S., Tsutsui, H., Shiina, K., Sprunck, S., Takeuchi, H., Yui, R., Kasahara, R. D., Hamamura, Y., Mizukami, A., Susaki, D., et al. (2009). Defensin-like polypeptide LUREs are pollen tube attractants secreted from synergid cells. *Nature* **458**, 357-361. doi:10.1038/nature07882
- Pierik, R., Tholen, D., Poorter, H., Visser, E. J. W. and Voesenek, L. A. (2006). The Janus face of ethylene: growth inhibition and stimulation. *Trends Plant Sci.* **11**, 176-183. doi:10.1016/j.tplants.2006.02.006
- Qiu, Y.-L., Li, L., Wang, B., Chen, Z., Knoop, V., Groth-Malonek, M., Dombrowska, O., Lee, J., Kent, L., Rest, J. et al. (2006). The deepest divergences in land plants inferred from phylogenomic evidence. *Proc. Natl. Acad. Sci. USA* **103**, 15511-15516. doi:10.1073/pnas.0603335103
- Richter, J., Ploderer, M., Mongelard, G., Gutierrez, L. and Hauser, M.-T. (2017). Role of CrRLK1L cell wall sensors HERCULES1 and 2, THESEUS1, and FERONIA in growth adaptation triggered by heavy metals and trace elements. *Front. Plant Sci.* **8**, 1554. doi:10.3389/fpls.2017.01554
- Richter, J., Watson, J. M., Stasnik, P., Borowska, M., Neuhold, J., Berger, M., Stolt-Bergner, P., Schoft, V. and Hauser, M.-T. (2018). Multiplex mutagenesis of four clustered CrRLK1L with CRISPR/Cas9 exposes their growth regulatory roles in response to metal ions. *Sci. Rep.* **8**, 12182. doi:10.1038/s41598-018-30711-3
- Rotman, N., Rozier, F., Boavida, L., Dumas, C., Berger, F. and Faure, J.-E. (2003). Female control of male gamete delivery during fertilization in *Arabidopsis thaliana*. *Curr. Biol.* **13**, 432-436. doi:10.1016/S0960-9822(03)00993-9
- Rövekamp, M., Bowman, J. L. and Grossniklaus, U. (2014). Back to the rhizoids of plant sexual development. *23rd Int. Congr. Sex. Plant Reprod. Porto*

- Port., p. 132. <https://www.fc.up.pt/sprporto2014/doc/23rd%20International%20congress%20on%20sexual%20plant%20reproduction%20ABSBook.pdf>.
- Rövekamp, M., Bowman, J. L. and Grossniklaus, U.** (2016). *Marchantia* MpRKD regulates the gametophyte-sporophyte transition by keeping egg cells quiescent in the absence of fertilization. *Curr. Biol.* **26**, 1782-1789. doi:10.1016/j.cub.2016.05.028
- Sachs, A. B. and Varani, G.** (2000). Eukaryotic translation initiation: there are (at least) two sides to every story. *Nat. Struct. Biol.* **7**, 356-361. doi:10.1038/75120
- Schindelin, J., Arganda-Carreras, I., Frise, E., Kaynig, V., Longair, M., Pietzsch, T., Preibisch, S., Rueden, C., Saalfeld, S., Schmid, B. et al.** (2012). Fiji: An open-source platform for biological-image analysis. *Nat. Methods* **9**, 676-682. doi:10.1038/nmeth.2019
- Schoenaers, S., Balcerowicz, D., Breen, G., Hill, K., Zdanio, M., Mouille, G., Holman, T. J., Oh, J., Wilson, M. H., Nikonorova, N. et al.** (2018). The auxin-regulated CrRLK1L kinase ERULUS controls cell wall composition during root hair tip growth. *Curr. Biol.* **28**, 722-732. doi:10.1016/j.cub.2018.01.050
- Schulze-Muth, P., Irmiler, S., Schröder, G. and Schröder, J.** (1996). Novel type of receptor-like protein kinase from a higher plant (*Catharanthus roseus*): cDNA, gene, intramolecular autophosphorylation, and identification of a threonine important for auto- and substrate phosphorylation. *J. Biol. Chem.* **271**, 26684-26689. doi:10.1074/jbc.271.43.26684
- Schwede, T., Kopp, J., Guex, N. and Peitsch, M. C.** (2003). SWISS-MODEL: an automated protein homology-modeling server. *Nucleic Acids Res.* **31**, 3381-3385. doi:10.1093/nar/gkg520
- Shih, H.-W., Miller, N. D., Dai, C., Spalding, E. P. and Monshausen, G. B.** (2014). The receptor-like kinase FERONIA is required for mechanical signal transduction in *Arabidopsis* seedlings. *Curr. Biol.* **24**, 1887-1892. doi:10.1016/j.cub.2014.06.064
- Shiu, S. H. and Bleeker, A. B.** (2001). Plant receptor-like kinase gene family: diversity, function, and signaling. *Sci. STKE* **2001**, re22. doi:10.1126/stke.2001.113.re22
- Showalter, A. M.** (1993). Structure and function of plant cell wall proteins. *Plant Cell* **5**, 9-23. doi:10.1105/tpc.5.1.9
- Solly, J. E., Cunniffe, N. J. and Harrison, C. J.** (2017). Regional growth rate differences specified by apical notch activities regulate liverwort thallus shape. *Curr. Biol.* **27**, 16-26. doi:10.1016/j.cub.2016.10.056
- Srivastava, R., Liu, J.-X., Guo, H., Yin, Y. and Howell, S. H.** (2009). Regulation and processing of a plant peptide hormone, AtRALF23, in *Arabidopsis*. *Plant J.* **59**, 930-939. doi:10.1111/j.1365-313X.2009.03926.x
- Stegmann, M., Monaghan, J., Smakowska-Luzan, E., Rovenich, H., Lehner, A., Holton, N., Belkhadir, Y. and Zipfel, C.** (2017). The receptor kinase FER is a RALF-regulated scaffold controlling plant immune signaling. *Science* **355**, 287-289. doi:10.1126/science.aal2541
- Steinwand, B. J. and Kieber, J. J.** (2010). The role of receptor-like kinases in regulating cell wall function. *Plant Physiol.* **153**, 479-484. doi:10.1104/pp.110.155887
- Tang, W., Lin, W., Zhou, X., Guo, J., Dang, X., Li, B., Lin, D. and Yang, Z.** (2021). Mechano-transduction via the pectin-FERONIA complex activates ROP6 GTPase signaling in *Arabidopsis* pavement cell morphogenesis. *Curr. Biol.* **S0960-9822**, 01590-01596.
- Trapnell, C., Pachter, L. and Salzberg, S. L.** (2009). TopHat: discovering splice junctions with RNA-Seq. *Bioinformatics* **25**, 1105-1111. doi:10.1093/bioinformatics/btp120
- Vandesompele, J., De Preter, K., Pattyn, F., Poppe, B., Van Roy, N., De Paepe, A. and Speleman, F.** (2002). Accurate normalization of real-time quantitative RT-PCR data by geometric averaging of multiple internal control genes. *Genome Biol.* **3**, RESEARCH0034. doi:10.1186/gb-2002-3-7-research0034
- Vogler, H., Draeger, C., Weber, A., Felekis, D., Eichenberger, C., Routier-Kierzkowska, A.-L., Boisson-Dernier, A., Ringli, C., Nelson, B. J., Smith, R. S., et al.** (2013). The pollen tube: a soft shell with a hard core. *Plant J.* **73**, 617-627. doi:10.1111/tj.12061
- Westermann, J., Streubel, S., Franck, C. M., Lentz, R., Dolan, L. and Boisson-Dernier, A.** (2019). An evolutionarily conserved receptor-like kinases signaling module controls cell wall integrity during tip growth. *Curr. Biol.* **29**, 4153. doi:10.1016/j.cub.2019.11.010
- Wickett, N. J., Mirarab, S., Nguyen, N., Warnow, T., Carpenter, E., Matasci, N., Ayyampalayam, S., Barker, M. S., Burleigh, J. G., Gitzendanner, M. A. et al.** (2014). Phylotranscriptomic analysis of the origin and early diversification of land plants. *Proc. Natl. Acad. Sci. USA* **111**, E4859-E4868. doi:10.1073/pnas.1323926111
- Wickham, H.** (2016). *ggplot2: elegant graphics for data analysis*. Springer.
- Wolf, S. and Höfte, H.** (2014). Growth control: a saga of cell walls, ROS, and peptide receptors. *Plant Cell* **26**, 1848-1856. doi:10.1105/tpc.114.125518
- Wolf, S., Hématy, K. and Höfte, H.** (2012). Growth control and cell wall signaling in plants. *Annu. Rev. Plant Biol.* **63**, 381-407. doi:10.1146/annurev-arplant-042811-105449
- Xiao, Y., Stegmann, M., Han, Z., DeFalco, T. A., Parys, K., Xu, L., Belkhadir, Y., Zipfel, C. and Chai, J.** (2019). Mechanisms of RALF peptide perception by a heterotypic receptor complex. *Nature* **572**, 270-274. doi:10.1038/s41586-019-1409-7
- Yu, F., Qian, L., Nibau, C., Duan, Q., Kita, D., Levasseur, K., Li, X., Lu, C., Li, H., Hou, C. et al.** (2012). FERONIA receptor kinase pathway suppresses abscisic acid signaling in *Arabidopsis* by activating ABI2 phosphatase. *Proc. Natl. Acad. Sci. USA* **109**, 14693-14698. doi:10.1073/pnas.1212547109
- Zhu, L., Chu, L.-C., Liang, Y., Zhang, X.-Q., Chen, L.-Q. and Ye, D.** (2018). The *Arabidopsis* CrRLK1L protein kinases BUPS1 and BUPS2 are required for normal growth of pollen tubes in the pistil. *Plant J.* **95**, 474-486. doi:10.1111/tj.13963
- Zhu, S., Fu, Q., Xu, F., Zheng, H. and Yu, F.** (2021). New paradigms in cell adaptation: decades of discoveries on the CrRLK1L receptor kinase signalling network. *New Phytol.* **232**, 1168-1183. doi:10.1111/nph.17683
- Zuker, M.** (2003). Mfold web server for nucleic acid folding and hybridization prediction. *Nucleic Acids Res.* **31**, 3406-3415. doi:10.1093/nar/gkg595

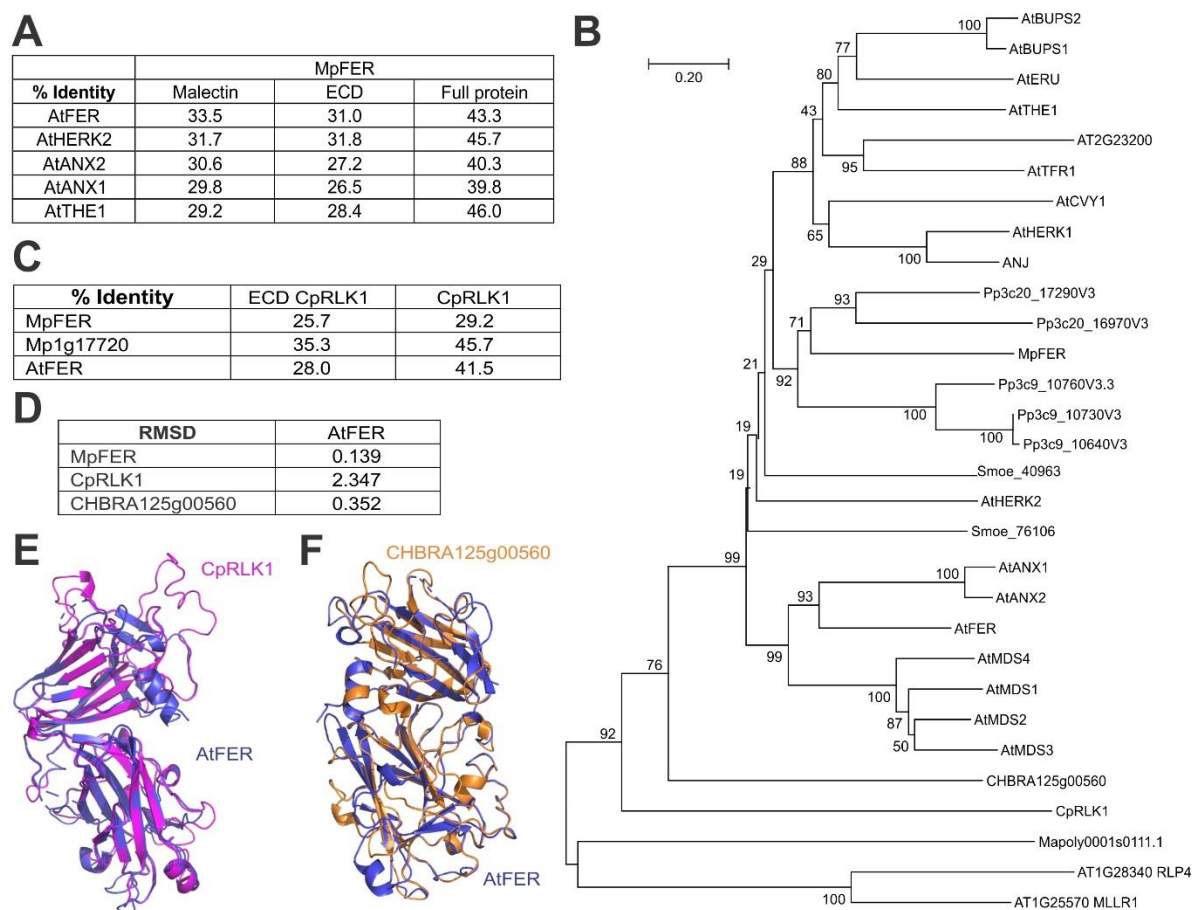


Fig. S1. The CrRLK1L Family Appeared together with Land Plants. Related to Fig. 1.

(A) Percentage of identity of the malectin-like domain, the complete ECD, and the full protein of MpFER with AtFER, AtHERK2, AtANX2, AtANX1, and AtTHE1.

(B) A rooted neighbour-joining tree of the amino acid sequence of the predicted malectin-like domains was generated using ClustalW. CrRLK1L members from *Marchantia polymorpha* (Mp), *Physcomitrium patens* (Pp), *Selaginella moellendorffii* (Smoe), and *Arabidopsis thaliana* (At) were used. Algal CpRLK1 and CHBRA125g00560, as well as Mp1g17720 (Mapoly001s0111) were also included. The numbers indicate the bootstrap values (%) from 1000 replications. The given scale represents a substitution frequency of 0.1 amino acids per site.

(C) Percentage of identity of the ECD and full protein of CpRLK1 with MpFER, AtFER, and Mp1g17720 (Mapoly001s0111).

(D) RMSD values for prediction of MpFER, CpRLK1, and CHBRA125g00560 3D structures of the ECD based on the AtFER ECD.

(E) Structural superposition of the ECD of AtFER (blue) and CpRLK1 (purple).

(F) Structural superposition of the ECD of AtFER (blue) and CHBRA125g00560 (orange) from *Chara brunii*.

A *Mp*miR160 Mp1g26670
 GCACCTCTCTCTCCGACTGCAGCCCGTTTTTCGAGATCCGAGGACTTGCTCGACGCGACTAATTGGGGAGGCCAGACTG
 CACTT**GCCTGGCTCCCTGTATGCCAACT**GTAGGAGCTCCTCAGAGACCTTGACAGGCTCCGTAGCTGGCATT**CAGGGGG**
CCATGCAGGAGGAAAGTCGCTACCTCCCGCAAGGTGCGACTAGCTTTCTGTCTTGGGTGCACACCTCACTGATGTTTGA
 TAGATTTACTTA

amiR-Mp*FER*1
TGCAAGCTTGCACCTCTCTCTCCGACTGCAGCCCGTTTTTCGAGATCCGAGGACTTGCTCGACGCGACTAATTGGGGAG
 GCCAGACTGCAC**TGACGTAGGCAAACTTGTCTGAACT**GTAGGAGCTCCTCAGAGACCTTGACAGGCTCCGTAGCT**CGAC**
ATGTTTTGTCTACCTCAGGAGGAAGTCGCTACCTCCCGCAAGGTGCGACTAGCTTTCTGTCTTGGGTGCACACCTCACT
 GATGTTT**GATAGATTTACTTAGGATCCATA**

amiR-Mp*FER*2
TGCAAGCTTGCACCTCTCTCTCCGACTGCAGCCCGTTTTTCGAGATCCGAGGACTTGCTCGACGCGACTAATTGGGGAG
 GCCAGACTGCAC**TTCGATGTTCGAAAATCCAGGT**GACTGTAGGAGCTCCTCAGAGACCTTGACAGGCTCCGTAGCCACCT
GCATTTTTTGCACAACGAGGAGGAAGTCGCTACCTCCCGCAAGGTGCGACTAGCTTTCTGTCTTGGGTGCACACCTCACT
 GATGTTT**GATAGATTTACTTAGGATCCATA**

amiR-Mp*FER*3
TGCAAGCTTGCACCTCTCTCTCCGACTGCAGCCCGTTTTTCGAGATCCGAGGACTTGCTCGACGCGACTAATTGGGGAG
 GCCAGACTGCAC**TCCGAACTTCTCAGAGACT**CACTGTAGGAGCTCCTCAGAGACCTTGACAGGCTCCGTAGCGAG**TC**
TGTGAGGGAGTTGGGAGGAGGAAGTCGCTACCTCCCGCAAGGTGCGACTAGCTTTCTGTCTTGGGTGCACACCTCACT
 GATGTTT**GATAGATTTACTTAGGATCCATA**

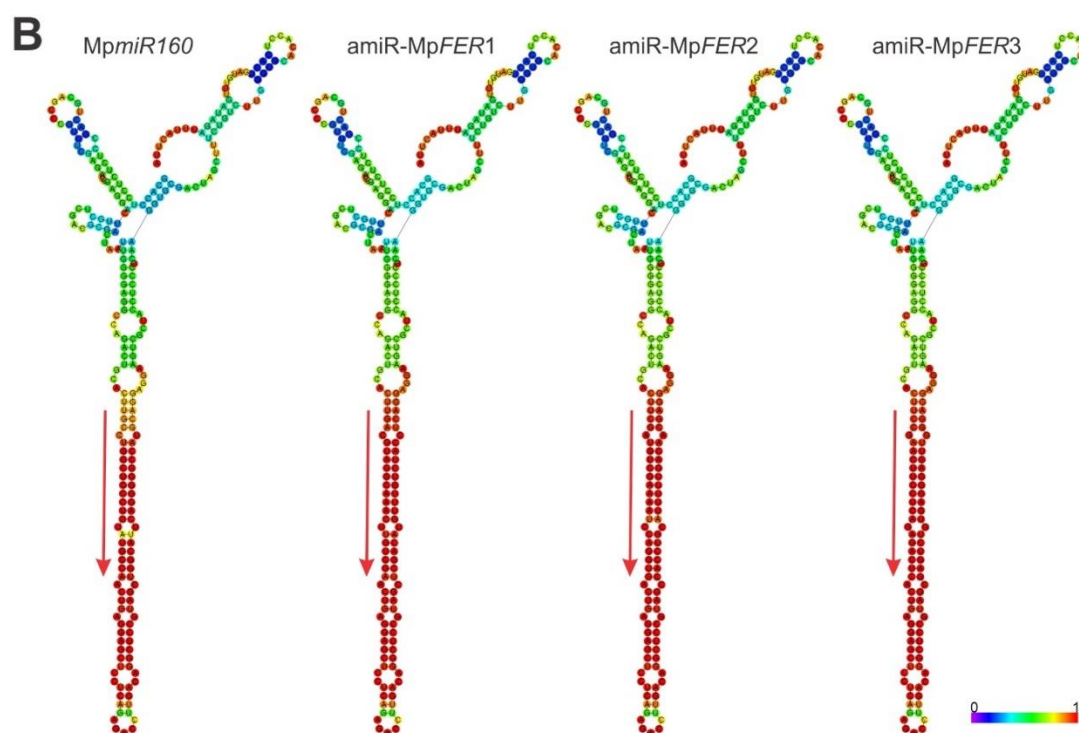


Fig. S2. Design of amiR-Mp*FER* Precursors. Related to Fig. 3.

(A) *Mp*miR160 (Mapoly0002s0211, Mp1g26670) and amiR-Mp*FER*1, amiR-Mp*FER*2, and amiR-Mp*FER*3 sequences. miRNA sequences are in red and miRNA* in blue. Cloning sequences from amiR-Mp*FER* constructs are in bold.

(B) Drawing of the minimum free energy structure of *Mp*miR160 and amiR-Mp*FER*3 constructs predicted by the RNAfold web server (<http://rna.tbi.univie.ac.at/cgi->

[bin/RNAWebSuite/RNAfold.cgi](#)). Red arrows indicate location and orientation of the mature miRNA in the precursor. The structures are coloured by base-pairing probabilities; for unpaired regions the colour denotes the probability of being unpaired.

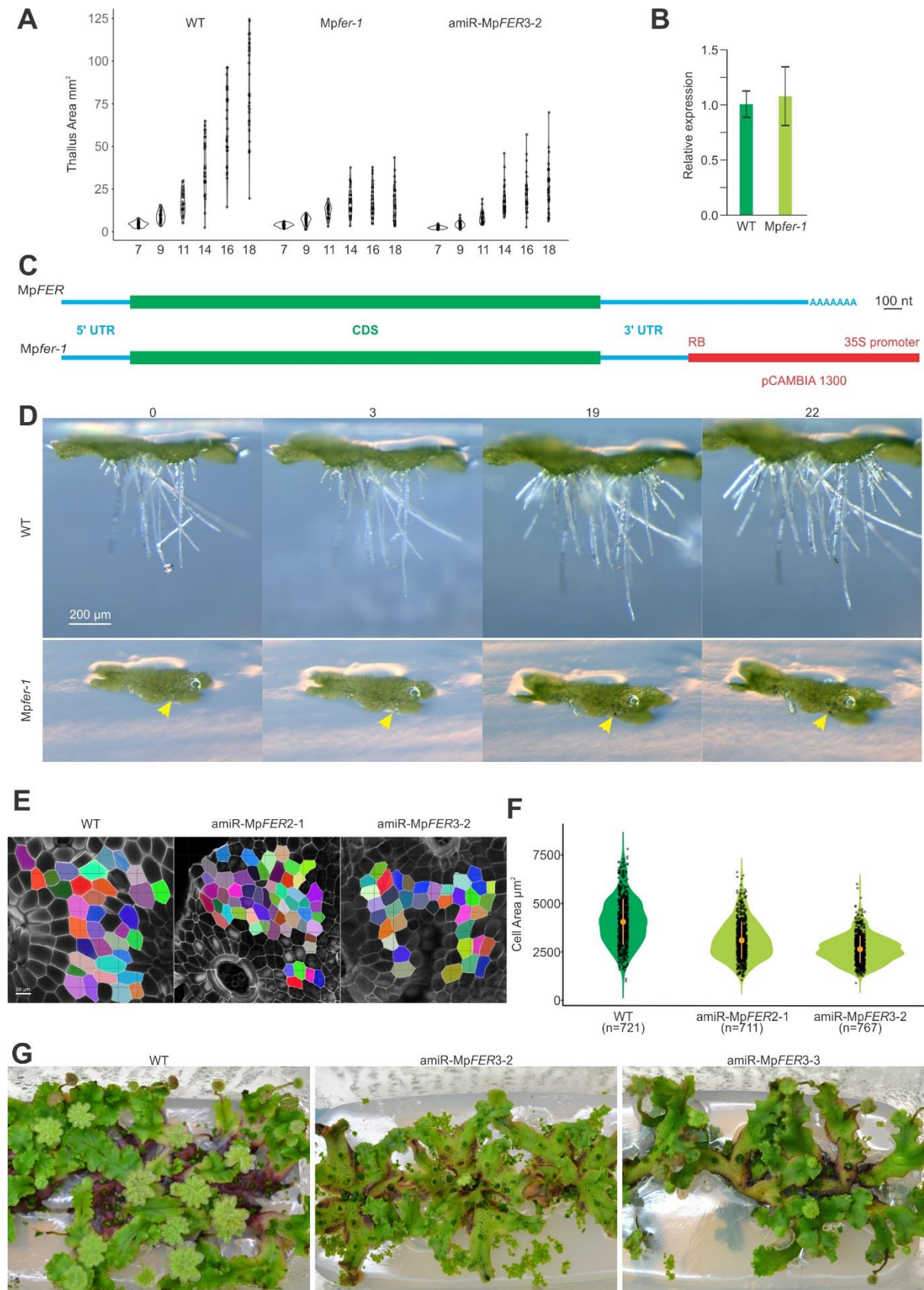


Fig. S3. Reduction in Thallus and Cell Area in Plants with Reduced *MpFER* Levels. Related to Figs. 3 and 5.

(A) Violin plot of thallus area of wild-type (WT), *Mpfer-1*, and *amiR-MpFER3-2* plants at different days after putting gemmae on plates. $n = 30$. Areas were estimated using ImageJ software.

(B) Relative expression level of *MpFER* in 14 day-old WT and *Mpfer-1* gemmalings, as measured by qRT-PCR. *MpEF1* was used as internal control. Shown are means \pm standard error of the mean (SEM) of three biological replicates. Statistical analysis was performed by a one-way analysis of variance (ANOVA) follow by a post-hoc Duncan test, no significant difference was observed.

(C) Schematic of *MpFER* transcripts in WT (upper) and *Mpfer-1* plants (lower).

(D) Pictures of growing rhizoids at different time points (in h). Yellow arrows indicate a growing rhizoid in *Mpfer-1* line that burst between 3 and 19 h.

(E) Representative images from cell surface areas measured in WT, *amiR-MpFER2-1*, and *amiR-MpFER3-2* plants. Scale bar, 50 μm .

(F) Violin plot of cell areas of WT, *amiR-MpFER2-1*, and *amiR-MpFER3-2* plants. Difference is significant based on the nonparametric Kruskal-Wallis test and a linear regression model with a highly significant interaction ($p < 0.001$). Orange circles indicate the group mean and the corresponding vertical bars the standard deviation for each group.

(G) Induction of antheridiophores in WT and two independent *amiR-MpFER3* lines. Three plants were grown in each sterile plastic box under far-red light induction.

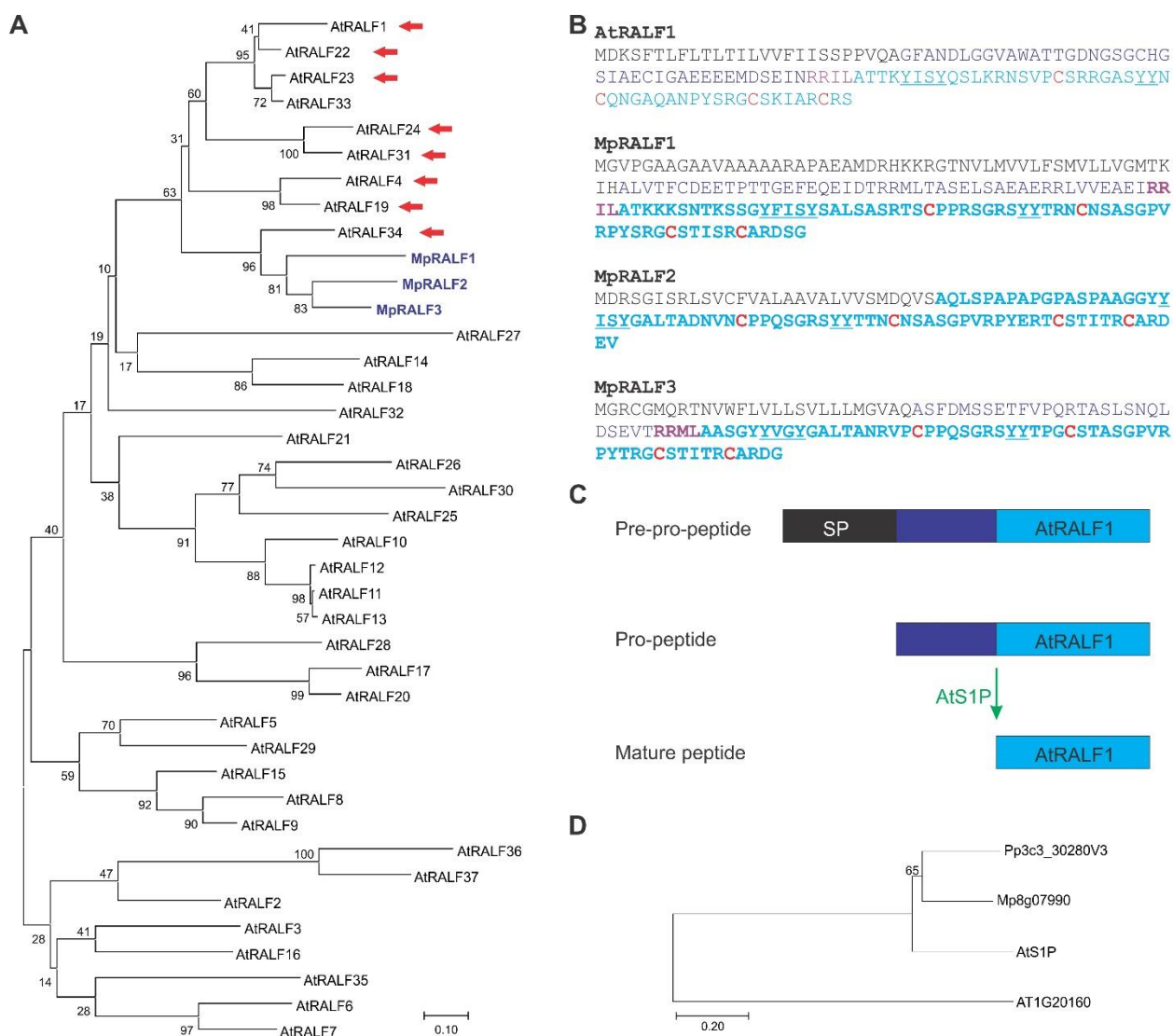


Fig. S4. MpRALF Peptides Belong to the AtRALF1-clade of the RALF Family.

Related to Fig. 6.

(A) A rooted neighbour-joining tree of the amino acid sequence of the predicted mature RALF peptides was generated using ClustalW. RALF members from *M. polymorpha* and *A. thaliana* were used. Red arrows indicate RALFs that are known ligands of CrRLK1Ls. The numbers indicate the bootstrap values (%) from 1000 replications. The given scale represents a substitution frequency of 0.1 amino acids per site.

(B) Amino acid sequence comparison of AtRALF1 and MpRALF1-3. Predicted signal peptides are in black, predicted mature peptides in light blue, conserved Cys in red, and predicted S1P recognition sites in violet.

(C) Processing pathway AtRALF1 by the S1P protease.

(D) A rooted neighbour-joining tree of the amino acid sequence of the S1P orthologs was generated using ClustalW. S1P members from *M. polymorpha*, *P. patens*, and *A. thaliana* were used. The numbers indicate the bootstrap values (%) from 1000 replications. The given scale represents a substitution frequency of 0.1 amino acids per site.

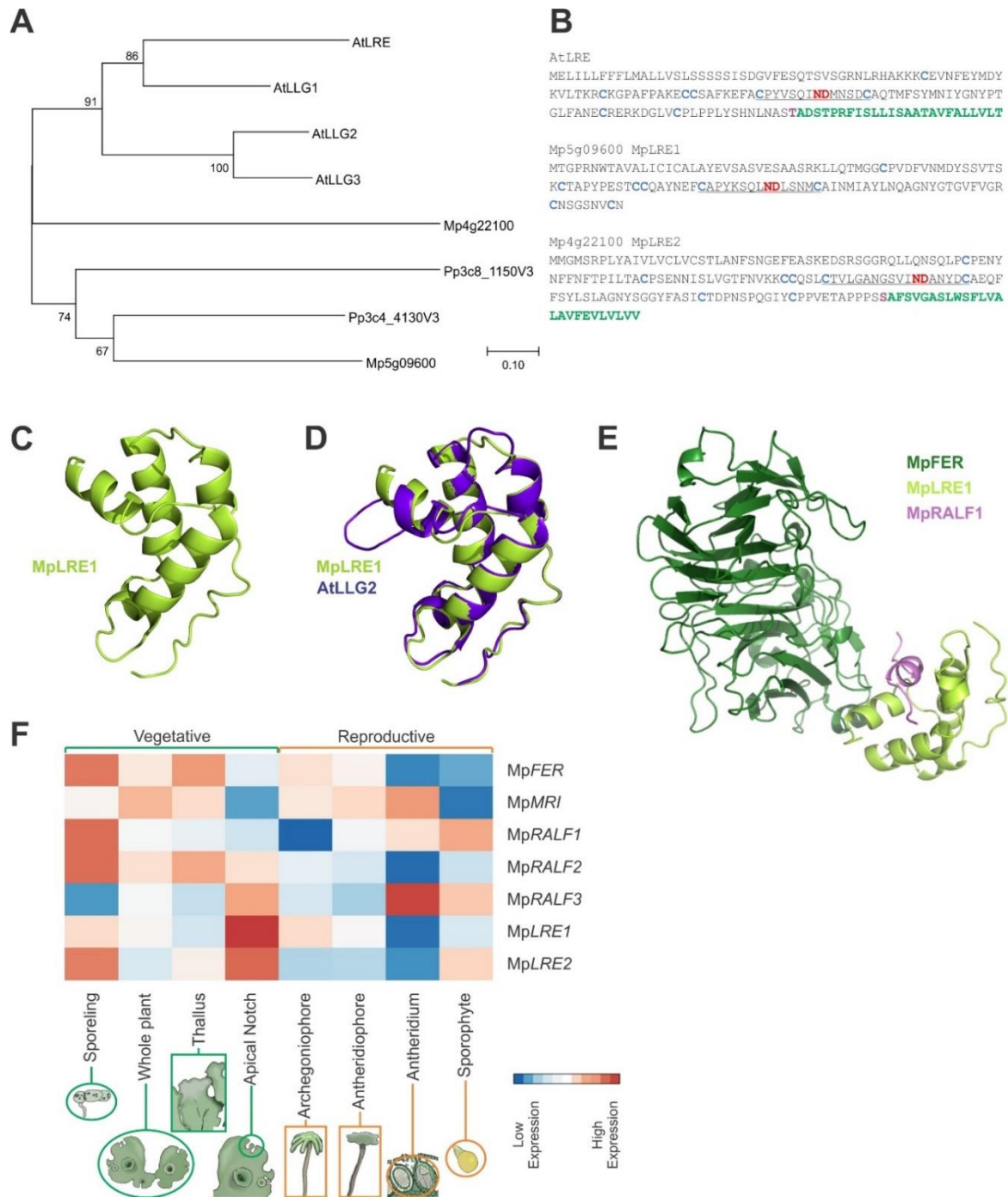


Fig. S5. Two LORELEI-like Proteins Are Encoded in the *M. polymorpha* Genome. Related to Fig. 6.

(A) A rooted neighbor-joining tree of the amino acid sequence of LRE orthologs was generated using ClustalW. LRE members from *M. polymorpha*, *P. patens*, and *A.*

thaliana were used. The numbers indicate the bootstrap values (%) from 1000 replications. The given scale represents a substitution frequency of 0.1 amino acids per site.

(B) Amino acid sequence of AtLRE, MpLRE1, and MpLRE2. Conserved Cys are in light blue, the ND motif in red, and the GPI-anchoring site in green.

(C) Cartoon representation of the predicted 3-dimensional structure of MpLRE1, showing predicted alpha-helices.

(D) Structural superposition of AtLGG2 (blue) and MpLRE1 (green).

(E) Cartoon representation of the predicted 3-dimensional structure of the MpFER/MpLRE1/MpRALF1 complex, showing predicted alpha-helices and beta-sheets.

(F) Heatmap depicting relative gene expression based on RNAseq data (row-Z-score of vs normalized counts) of MpFER and the *M. polymorpha* orthologs of AtMRI, AtRALF1, and AtLRE across different tissues. Vegetative and reproductive tissues are grouped by green and orange, respectively. Averaged expression values are represented with colours of increasing red and blue intensity indicating upregulation and downregulation of gene expression, respectively.

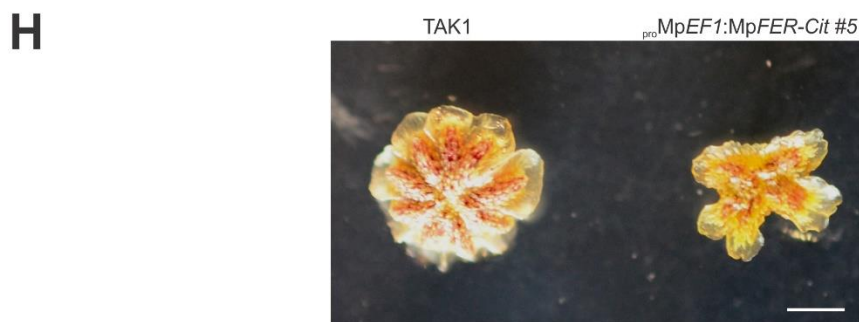
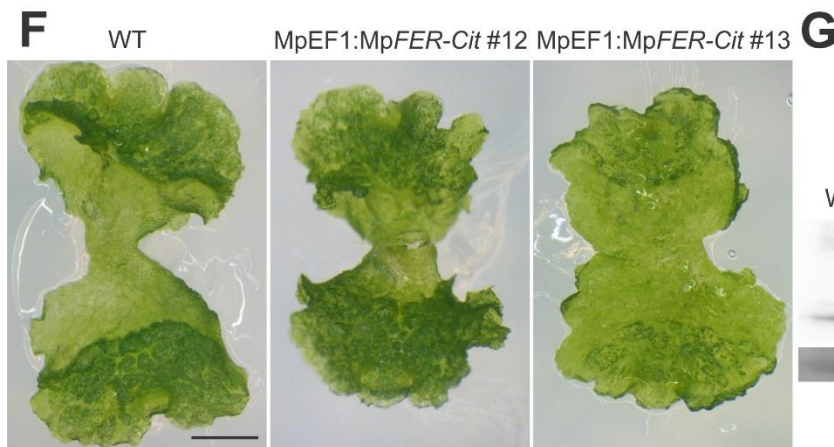
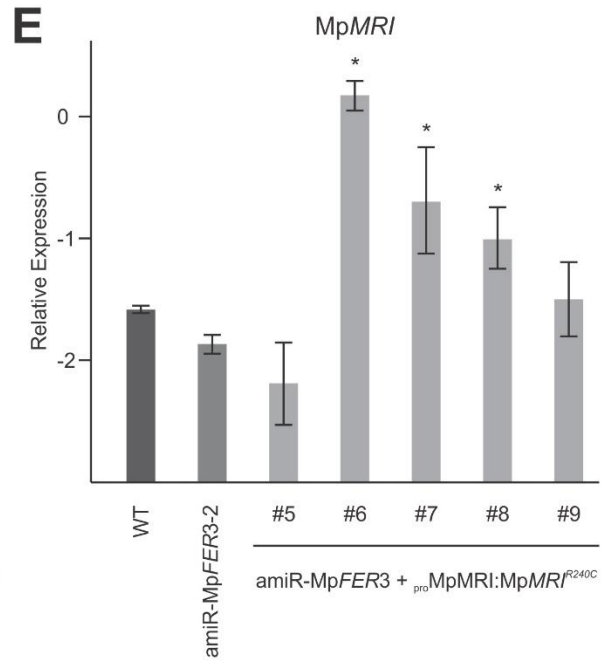
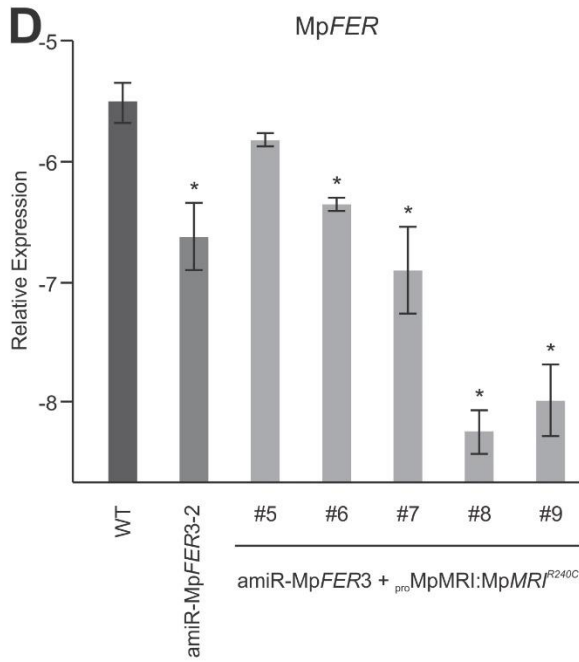
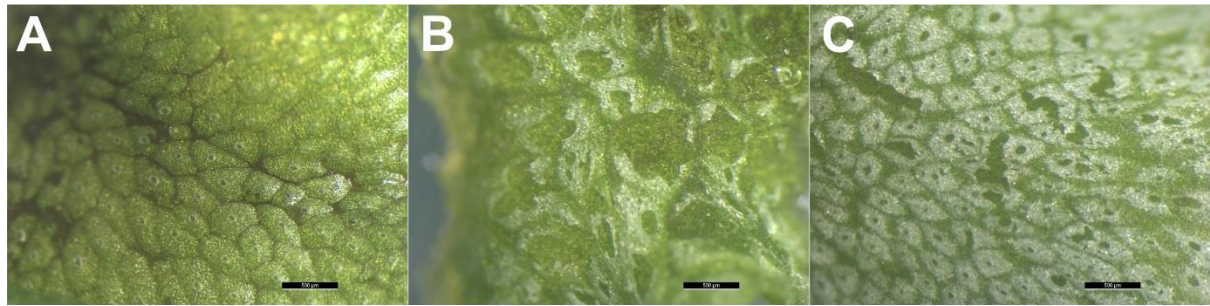


Fig. S6. Expression of MpMRI^{R240C} Suppresses the Bursted Rhizoid Phenotype of amiR-MpFER3 Lines but Leads to Aberrant Epidermis Development. Related to Figs. 6,7.

(A to C) Epidemical pictures of thalli from the wild-type (WT) (A), and amiR-MpFER3 + *pro*MpMRI:MpMRI^{R240C} lines #6 (B) and #8 (C), which both partially suppressed the bursting rhizoid phenotype (Fig. 6).

(D and E) Relative expression of MpFER (D) and MpMRI (E) against the geometric mean of the reference genes MpACT1, MpACT7, and MpAPT3 in WT, amiR-MpFER3-2, and 5 lines (#5 to #9) co-transformed with the amiR-MpFER3-2 and *pro*MpMRI:MpMRI^{R240C} constructs. Expression levels of three biological replicates were assessed by droplet digital PCR (ddPCR). The y-axis corresponds to the log₂-ratio between the test and the geometric mean of the reference genes. Shown are means ± SEMs of three biological replicates. Statistical analysis was performed by one-way analysis of variance (ANOVA) followed by a post-hoc Duncan test (*P < 0.01).

(F) Representative pictures of 10-day old gemmalings of wild-type (WT) and two different lines overexpressing MpFER (*pro*MpEF1:MpFER-Cit). Scale bar, 1 mm.

(G) Western blot analysis of *pro*MpEF1:MpFER-Cit lines from Fig. S6A using an anti-GFP antibody. WT lines were used as negative controls. The Ponceau membrane staining of the most intense band at 55 kDa (presumably Rubisco) was used as a loading control.

(H) Representative images of the antheridial receptacle of WT and *pro*MpEF1:MpFER-Cit plants. Scale bar, 2 mm.

Table S1. Primer sequences used for qRT-PCR, ddPCR, and 3' RACE-PCR

Name	Sequence
Mp <i>FER</i>	CGAGGAGCATTGCGAGATG
Mp <i>FER</i>	AGGTCGGTGCCGTAGAGATG
Mp <i>EF1α</i>	AGGTTGTCACCATGGGAAAGGAGA
Mp <i>EF1α</i>	TCACACGCTTGCAATACCTCCCA
Mp <i>MRI</i>	TGGCAGCTCGTCTCCACTCT
Mp <i>MRI</i>	AGTCATGGCGTACTCGGGTG
Mp <i>ACT7</i>	AGGCATCTGGTATCCACGAG
Mp <i>ACT7</i>	ACATGGTCGTTCTCCAGAC
Mp <i>ACT1</i>	GAGCGCGGTTACTCTTTTAC
Mp <i>ACT1</i>	GACCGTCAGGAAGCTCGTAG
Mp <i>APT3</i>	CGACATGGACGGCCTGGAGCTGGAG
Mp <i>APT3</i>	CGAAAGCCCAAGAAGCTACC
Mp <i>APT3</i>	GTACCCCGGTTGCAATAAG
3'RACE-Fwd1	AACGGTGTTGGATGGTTCGATTAG
3'RACE-Fwd2	
Oligo(dC)	CCCCCCCCCCCCCCCCCVN

Table S2. List of primers used for cloning

Name	Target	Sequence
proMp <i>FER</i> F	Mp <i>FER</i>	TAGTTGGAATGGGTTTCAATGCTGTGCGACCACTGACTTC
proMp <i>FER</i> R	Mp <i>FER</i>	TTATGGAGTTGGGTTTCAAGTAGTGTATCCTCCAGCCGCTTT
Mp <i>FER</i> F	Mp <i>FER</i>	GGGGACAAGTTTGTACAAAAAAGCAGGCT- AGAGCCCAAGGAGGAAGGGCGACCA
Mp <i>FER</i> R	Mp <i>FER</i>	GGGGACCACTTTGTACAAGAAAGCTGGGTT- CCTTCCTTGAGGGTTCACCAGCTG

Table S3. List of publicly available RNA-seq samples downloaded from SRA and used in this study. Sample list of publicly available RNA-seq samples that were used in this study.

The table also includes the tissue classification in which every sample was grouped with, their corresponding phase (vegetative vs sexual), and the genotype they correspond to. BC = Back Crossed to TAK1 genotype followed by the number of back crosses.

SRR_ID	SRX_ID	Organism	Tissue Group	Phase	Strain
SRR896228	SRX301558	M.Polymorpha;WT	Thallus	Vegetative	Tak1
SRR896225	SRX301555	M.Polymorpha;WT	Archegoniophore	Sexual	Tak2BC4
SRR896226	SRX301560	M.Polymorpha;WT	Thallus	Vegetative	Tak1
SRR896229	SRX301557	M.Polymorpha;WT	Thallus	Vegetative	Tak1
SRR896224	SRX301559	M.Polymorpha;WT	Sporeling	Vegetative	Tak1xTak2BC4
SRR896230	SRX301553	M.Polymorpha;WT	Antheridiophore	Sexual	Tak1
SRR896227	SRX301554	M.Polymorpha;WT	Thallus	Vegetative	Tak1xTak2BC4
SRR896223	SRX301556	M.Polymorpha;WT	Sporophyte	Sexual	Tak1xTak2BC4
SRR971246	SRX346276	M.Polymorpha;WT	Archegoniophore	Sexual	Tak2
SRR971244	SRX346274	M.Polymorpha;WT	Thallus	Vegetative	Tak2
SRR971248	SRX346277	M.Polymorpha;WT	Antheridiophore	Sexual	Tak1
SRR971249	SRX346278	M.Polymorpha;WT	Archegoniophore	Sexual	Tak2
SRR971243	SRX346272	M.Polymorpha;WT	Thallus	Vegetative	Tak1
SRR971245	SRX346275	M.Polymorpha;WT	Antheridiophore	Sexual	Tak1
SRR1553299	SRX682817	M.Polymorpha;WT	Sporophyte	Sexual	Tak1xTak2
SRR1552617	SRX682160	M.Polymorpha;WT	Whole_Plant	Vegetative	Tak1xTak2
SRR1553294	SRX682811	M.Polymorpha;WT	Apical_Notch	Vegetative	Tak1xTak2
SRR1553297	SRX682815	M.Polymorpha;WT	Sporophyte	Sexual	Tak1xTak2
SRR1553296	SRX682814	M.Polymorpha;WT	Apical_Notch	Vegetative	Tak1xTak2
SRR1553276	SRX682793	M.Polymorpha;WT	Whole_Plant	Vegetative	Tak1xTak2
SRR1553295	SRX682813	M.Polymorpha;WT	Apical_Notch	Vegetative	Tak1xTak2
SRR1553298	SRX682816	M.Polymorpha;WT	Sporophyte	Sexual	Tak1xTak2
DRR050343	DRX045349	M.Polymorpha;WT	Whole_Plant	Vegetative	Tak1xTak2
DRR050346	DRX045352	M.Polymorpha;WT	Antheridiophore	Sexual	Tak1xTak2
DRR050347	DRX045353	M.Polymorpha;WT	Antheridiophore	Sexual	Tak1xTak2
DRR050348	DRX045354	M.Polymorpha;WT	Antheridiophore	Sexual	Tak1xTak2
DRR050353	DRX045359	M.Polymorpha;WT	Archegoniophore	Sexual	Tak1xTak2
DRR050344	DRX045350	M.Polymorpha;WT	Whole_Plant	Vegetative	Tak1xTak2
DRR050351	DRX045357	M.Polymorpha;WT	Archegoniophore	Sexual	Tak1xTak2
DRR050349	DRX045355	M.Polymorpha;WT	Antheridium	Sexual	Tak1xTak2
DRR050352	DRX045358	M.Polymorpha;WT	Archegoniophore	Sexual	Tak1xTak2
DRR050345	DRX045351	M.Polymorpha;WT	Whole_Plant	Vegetative	Tak1xTak2
DRR050350	DRX045356	M.Polymorpha;WT	Antheridium	Sexual	Tak1xTak2
DRR118950	DRX111959	M.Polymorpha;WT	Whole_Plant	Vegetative	Tak1
DRR118945	DRX111954	M.Polymorpha;WT	Whole_Plant	Vegetative	Tak2BC3
DRR118951	DRX111960	M.Polymorpha;WT	Whole_Plant	Vegetative	Tak1
DRR118943	DRX111952	M.Polymorpha;WT	Whole_Plant	Vegetative	Tak2BC3
DRR118944	DRX111953	M.Polymorpha;WT	Whole_Plant	Vegetative	Tak2BC3
DRR118949	DRX111958	M.Polymorpha;WT	Whole_Plant	Vegetative	Tak1

Table S4. Quality estimation values generated during the modelling processes. For each target protein, several templates were considered for model comparison and validation. General Model Quality Estimate (GMQE) score and the QMEAN DisCo score are generated by SWISS-MODEL web server [60]: higher values indicate better accuracy in model prediction. RMSD stands for root-mean-square deviation and measures the average distance between the atoms of paired superimposed proteins, thus, the lower the values, the more similar is the modelled protein to the template.

Template Gene	Target Gene	Template PDB	GMQE	QMEAN DisCo	RMSD
AtFER	MpFER	6a5b.1.A	0.66	0.71 ± 0.05	0.139
AtANX1	MpFER	6fig.1.A	0.64	0.68 ± 0.05	0.144
AtANX2	MpFER	6fih.1.A	0.58	0.62 ± 0.05	0.104
AtLLG1	MpLRE1	6a5d.2.A	0.52	0.70 ± 0.10	0.11
AtLLG2	MpLRE1	6a5e.1.B	0.45	0.63 ± 0.11	0.14
AtLLG1	MpLRE2	6a5d.2.A	0.44	0.67 ± 0.05	0.15
AtLLG2	MpLRE2	6a5e.1.B	0.34	0.57 ± 0.09	0.18
AtFER	CpRLK1	6a5b.1.A	0.45	0.51 ± 0.05	2.347
AtANX1	CpRLK1	6fig.1.A	0.48	0.52 ± 0.05	3.038
AtANX2	CpRLK1	6fih.1.A	0.49	0.52 ± 0.05	1.721
AtFER	CHBRA125g00560	6a5b.1.A	0.58	0.61 ± 0.05	0.352
AtANX1	CHBRA125g00560	6fig.1.A	0.59	0.59 ± 0.05	0.41
AtANX2	CHBRA125g00560	6fih.1.A	0.59	0.59 ± 0.05	0.481